CFD SIMULATION OF VORTEX–INDUCED VIBRATIONS OF FREE SPAN PIPELINES INCLUDING PIPE-SOIL INTERACTIONS

A Thesis

by

FEI XIAO

Submitted to the Office of Graduate and Professional Studies of
Texas A&M University
in partial fulfillment of the requirements for the degree of

MASTER OF SCIENCE

Chair of Committee,	Hamn-Ching Chen
Committee Members,	Richard Mercier
	Robert Handler
Head of Department,	Robin Autenrieth

May 2015

Major Subject: Ocean Engineering

ABSTRACT

This paper presents a three dimensional numerical simulation of free span pipelines under vortex-induced vibrations (VIV) and pipe-soil interactions. Pipeline is simplified as a tensioned beam with uniformly distributed tension. The tensioned beam equations are solved using a fully implicit discretization scheme. The flow field around the pipeline is computed by numerically solving the unsteady Navier-Stokes equations. Fluid domain is discretized using overset grid system consists of several computational blocks and approximate one million grid points in total. Grid points in near-wall regions of pipeline and bottom are of high resolution, while far field flow is in relatively coarse grid. Fluid-structure interaction (FSI) is achieved by communicating forces and motions between fluid solver and pipeline motion solver. Pipeline motion solver inputs drag and lift forces calculated by fluid solver, then computes displacements in both in-line and cross-flow directions and outputs new positions of pipeline back to fluid solver. Soil effect also plays an important role in this simulation. The pipe-soil interactions are modeled as mass-spring system with equivalent stiffness.

Simulation results are compared with experiments for validation in three cases: (a) An isolated pipeline VIV in uniform current without boundary effect; (b) A pipeline horizontally placed close to plane boundary in uniform current at different gap to diameter ratios G/D; (c) A free span pipeline at specific gap-to-diameter ratio with respect to different reduced velocities.

DEDICATION

This thesis is dedicated to my girlfriend, Jane. Her encouragement and understanding have always been with me.

Also, this thesis is dedicated to my parents. Thanks for their persistent support, both mentally and financially.

ACKNOWLEDGEMENTS

I would like to thank my committee chair, Dr. Chen, and my committee members, Dr. Mercier and Dr. Handler, for their guidance and support throughout the course of this research.

Thanks also go to my friends and colleagues and the department faculty and staff for making my time at Texas A&M University a great experience. I also want to extend my gratitude to the Texas A&M University Supercomputer Center, which provided necessary facilities for my research work.

NOMENCLATURE

2D	Two Dimensional
3D	Three Dimensional
CFD	Computational Fluid Dynamics
D	Pipeline Outer Diameter
D_s	Pipeline Damping
DNS	Direct Numerical Simulation
E	Young's Modulus
EI	Bending stiffness
FANS	Finite-Analytic Navier-Stokes
f_n	Natural Frequency
FSI	Fluid-Structure Interaction
G	Gap Depth between Pipeline and Seabed
G/D	Gap to Diameter Ratio
I	Moment of Inertia
K_L	Soil Horizontal Dynamic Stiffness
K_V	Soil Vertical Dynamic Stiffness
L	Pipeline Overall Length
LES	Large Eddy Simulation
M	Pipeline Unit Mass
RANS	Reynolds-Averaged Navier-Stokes

RMS	Root Mean Square
T	Pipeline Axial Tension
U	Velocity of Current
ν	Poisson's ratio
VIV	Vortex-Induced Vibration

TABLE OF CONTENTS

Page

LIST OF FIGURES

Page

LIST OF TABLES

Page

CHAPTER I

INTRODUCTION AND LITERATURE REVIEW

Deep water pipelines are being laid on the seabed and used for offshore gas and oil transportation. Due to the unevenness of the seabed, part of a pipeline may become unsupported, which is called free span. A free span can also be caused by rock beams, artificial support, change of seabed topology and strudel scours (Veritas, 2006). As the currents passing by, periodic vortex shedding may lead to vortex-induced vibrations and finally cause fatigue damage (Blevins, 1977). Thus, predictions of VIV amplitude and frequency of free span pipelines are very important during the pipeline design process.

In the past several decades, offshore slender body VIV has been widely investigated based on both experimental and numerical studies. Trim et al. (2005) tested a long riser of L/D=1400 in uniform and linearly sheared current. Both bare riser and riser with strakes were evaluated in model tests. The suppression effectiveness of strakes was highly affected by percentage coverage. Tognarelli et al. (2008) conducted real dimension experiments in the Gulf of Mexico. The fatigue damage was evaluated under various conditions such as hung-off operations, connected operations and drilling operations. Lehn (2003) set up a model test for 10m long pipeline with diameter of 20mm. Different responses under varying current velocities were observed.

In recent years, numerical simulation played a more and more important role in offshore VIV problem due to the development of computational techniques, which is considered as a valuable alternative of experiments. Newman and Karniadakis (1996)

investigated the flow induced vibration of a flexible cable under Reynolds number of 100, 200 and 300. The parallel spectral element / Fourier method was consulted for solving the three-dimensional Navier–Stokes equations. Lucor et al. (2001) presented direct numerical simulation (DNS) results of flexible cylinder's VIV subjected to linear and exponential sheared flow. Vortex dislocations and force distribution have been discussed based on simulation results. Meneghini et al. (2004) studied the hydroelastic interactions between flexible cylinder and surrounding fluid. A computational efficiency discrete vortex method (DVM) was applied. Pontaza et al. (2004) studied circular cylinder freely vibration using an unsteady Reynolds-Averaged Navier-Stokes (RANS) method. Some of the results were computed by using large eddy simulation (LES). Huang et al. (2007, 2008, 2011) used a time domain Finite-Analytic Navier-Stokes (FANS) method to accomplish three-dimensional numerical simulation of riser VIV under various environment conditions.

Specifically, the VIV of a horizontal placed pipeline close to a plane boundary has been studied by several researchers. Bearman and Zdravkovich (1978) studied a circular cylinder placed at different heights above a plane boundary in wind tunnel. Smoke tunnel experiments were also included to visualize wake flow structures. Tsahalis (1983, 1984), Tsahalis and Jones (1981) discussed the influence of sea bottom proximity on VIV amplitude and frequency, as well as on the fatigue lives of suspended spans. Raghavan et al. (2009) tested influence of gap ratio over pipeline vibration amplitudes. Different phenomenon were observed at different gap to diameter ratios of $G/D<0.65$, $0.65<G/D<3.0$ and $G/D>3.0$. Most of these research works focused on experimental

study. The seabed gap-to-diameter ratio, G/D, is used for characterizing the effect of seabed proximity, where G is the distance between the seabed and the pipeline, and D is the outer diameter of the pipeline. In addition to effect of seabed proximity, pipe-soil interaction is another important factor that influences the oscillatory motion of pipelines. Yang et al. (2008) conducted experiments about VIV of a pipeline near an erodible sandy seabed. It was proved that free span pipeline VIV was highly influenced by the sand scour beneath the pipe.

In recent years, numerical methods began to take part in simulating VIV of free span pipelines. Tsukada and Morooka (2013) used a nonlinear Finite Element Method to solve a two dimensional problem by ignoring the motion in the in-line direction. Gamino et al. (2013) calculated fluid-structure interaction by using a partitioned approach. Pontaza et al. (2010) coupled a finite element model with computational fluid dynamics (CFD) code to study a free span pipeline attached to a pipeline end termination (PLET).

This paper presents a three dimensional numerical simulation of free span pipelines under VIV and pipe-soil interactions. Pipeline is simplified as a tensioned beam with uniformly distributed tension. It is solved using a fully implicit discretization scheme. The flow field around the pipeline is computed by numerically solving the unsteady Navier-Stokes equations. Fluid domain is discretized using overset grid system consists of several computational blocks and approximate one million grid points in total. Grid points in near-wall regions of pipeline and bottom are of high resolution, while far field flow is in relatively course grid. Fluid-structure interaction is achieved by communicating forces and motions between fluid solver and pipeline motion solver.

Pipeline motion solver inputs drag and lift forces calculated by fluid solver, then computes displacements in both in-line and cross-flow directions and outputs new positions of pipeline back to fluid solver. Soil effect also plays an important role in this simulation. The pipe-soil interactions are modeled as mass-spring system with equivalent stiffness.

Simulation results are compared with experiments for validation in three cases: (a) An isolated pipeline VIV in uniform current without bottom effect; (b) A straight pipeline horizontally placed close to plane boundary in uniform current, with different gap to diameter ratios G/D; (c) A free span pipeline VIV at specific gap-to-diameter ratio with respect to different reduced velocities.

CHAPTER II

NUMERICAL APPROACH

This Chapter introduces the numerical method for the pipeline VIV simulations, including structure motion solver development, CFD approach, fluid-structure interactions and soil model.

Pipeline Motion Solver

A deep water pipeline can be modeled as a tensioned beam in the in-line and cross-flow directions separately. The governing equations of a tensioned beam are described as:

$$T\frac{d^2y}{dx^2}+\frac{dy}{dx}\frac{dT}{dx}-\frac{d^2}{dx^2}\left(EI\frac{d^2y}{dx^2}\right)+F_y=M\ddot{y}+D_S\dot{y} \quad (1)$$

$$\mathrm{T}\frac{d^2z}{dx^2}+\frac{\mathrm{dz}}{\mathrm{dx}}\frac{dT}{dx}-\frac{d^2}{dx^2}\left(\mathrm{EI}\frac{d^2z}{dx^2}\right)+F_z=M\ddot{z}+D_S\dot{z} \quad (2)$$

Where *x* is the axial direction, *y* is the in-line direction, *z* is the cross-flow direction with the positive *z*-axis pointing upward, *T* is the axial tension, *E* is Young's modulus, *I* is the area moment of inertia, $\mathrm{F_y}$ and $\mathrm{F_z}$are the external forces in *y* and *z* directions, *M* is the mass of pipeline in unit length and D_S is the damping ratio. We apply finite difference scheme to discretize the governing equation in the in-line directions (discretization in the cross-flow direction follows the same scheme):

$$\frac{dy}{dx} = \frac{y_{j+1}^{n} - y_{j-1}^{n}}{2\Delta x}, \text{ For j=2…N-1,} \quad (3)$$

$$\frac{dy}{dx} = \frac{-3y_{j}^{n} + 4y_{j+1}^{n} - y_{j+2}^{n}}{2\Delta x}, \text{ For j=1,} \quad (4)$$

$$\frac{dy}{dx} = \frac{y_{j-2}^{n} - 4y_{j-1}^{n} + 3y_{j}^{n}}{2\Delta x}, \text{ For j=N,} \quad (5)$$

$$\frac{d^2y}{dx^2} = \frac{y_{j-1}^{n} - 2y_{j}^{n} + y_{j+1}^{n}}{\Delta x^2}, \text{ For j=2…N-1,} \quad (6)$$

$$\frac{d^2y}{dx^2} = \frac{y_{j}^{n} - 2y_{j+1}^{n} + y_{j+2}^{n}}{\Delta x^2}, \text{ For j=1,} \quad (7)$$

$$\frac{d^2y}{dx^2} = \frac{y_{j-2}^{n} - 2y_{j-1}^{n} + y_{j}^{n}}{\Delta x^2}, \text{ For j=N,} \quad (8)$$

$$\frac{d^4y}{dx^4} = \frac{y_{j-2}^{n} - 4y_{j-1}^{n} + 6y_{j}^{n} - 4y_{j+1}^{n} + y_{j+2}^{n}}{\Delta x^4}, \text{ For j=3…N-2,} \quad (9)$$

$$\frac{d^4y}{dx^4} = \frac{y_{j}^{n} - 4y_{j+1}^{n} + 6y_{j+2}^{n} - 4y_{j+3}^{n} + y_{j+4}^{n}}{\Delta x^4}, \text{ For j=1,} \quad (10)$$

$$\frac{d^4y}{dx^4} = \frac{y_{j-1}^{n} - 4y_{j}^{n} + 6y_{j+1}^{n} - 4y_{j+2}^{n} + y_{j+3}^{n}}{\Delta x^4}, \text{ For j=2,} \quad (11)$$

$$\frac{d^4y}{dx^4} = \frac{y_{j-3}^{n} - 4y_{j-2}^{n} + 6y_{j-1}^{n} - 4y_{j}^{n} + y_{j+1}^{n}}{\Delta x^4} \text{ For j=N-1,} \quad (12)$$

$$\frac{d^4y}{dx^4} = \frac{y_{j-4}^{n} - 4y_{j-3}^{n} + 6y_{j-2}^{n} - 4y_{j-1}^{n} + y_{j}^{n}}{\Delta x^4} \text{ For j=N,} \quad (13)$$

$$\ddot{y} = \frac{y_{j}^{n} - 2y_{j}^{n-1} + y_{j}^{n-2}}{\Delta t^2}, \text{ For n}\geq 3, \quad (14)$$

$\dot{y} = \frac{y_j^n - y_j^{n-1}}{\Delta t}$, For n≥2. (15)

For other parameters except y and z, we consider them as constant. The discretization results are presented as:

$$\frac{EI}{\Delta x^4} y_{j-2}^n - \left(\frac{T_j}{\Delta x^2} - \frac{1}{2\Delta x}\frac{dT_j}{dx} + \frac{4EI}{\Delta x^4}\right) y_{j-1}^n + \left(\frac{2T_j}{\Delta x^2} + \frac{6EI}{\Delta x^4} + \frac{M}{\Delta t^2} + \frac{D_S}{\Delta t}\right) y_j^n$$
$$- \left(\frac{T_j}{\Delta x^2} + \frac{1}{2\Delta x}\frac{dT_j}{dx} + \frac{4EI}{\Delta x^4}\right) y_{j+1}^n + \frac{EI}{\Delta x^4} y_{j+2}^n$$
$$= F_{yj}^n + \left(\frac{2M}{\Delta t^2} + \frac{D_S}{\Delta t}\right) y_j^{n-1} - \frac{M}{\Delta t^2} y_j^{n-2} \quad (16)$$

$$\frac{EI}{\Delta x^4} z_{j-2}^n - \left(\frac{T_j}{\Delta x^2} - \frac{1}{2\Delta x}\frac{dT_j}{dx} + \frac{4EI}{\Delta x^4}\right) z_{j-1}^n + \left(\frac{2T_j}{\Delta x^2} + \frac{6EI}{\Delta x^4} + \frac{M}{\Delta t^2} + \frac{D_S}{\Delta t}\right) z_j^n$$
$$- \left(\frac{T_j}{\Delta x^2} + \frac{1}{2\Delta x}\frac{dT_j}{dx} + \frac{4EI}{\Delta x^4}\right) z_{j+1}^n + \frac{EI}{\Delta x^4} z_{j+2}^n$$
$$= F_{zj}^n + \left(\frac{2M}{\Delta t^2} + \frac{D_S}{\Delta t}\right) z_j^{n-1} - \frac{M}{\Delta t^2} z_j^{n-2} \quad (17)$$

where Δx is the length off a pipeline element. In this study, we discretize the pipeline into N=200 elements. Δt is the time step, and *n* denotes current time step. The same discretization scheme is applied for solving pipeline motion in cross-flow direction. Parameters *T*, *EI*, *M*, D_S are specified at the beginning of the computation. External forces F_y and F_z are obtained from the fluid solver. The only unknowns are pipeline displacements at each computational node.

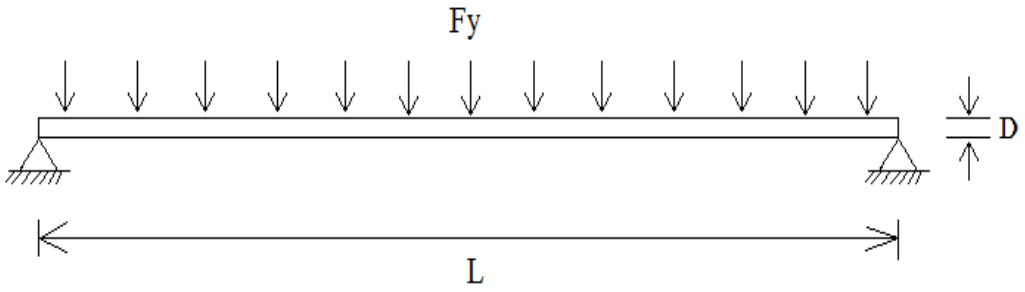

Figure 1 Static Validation Case for Pipeline Motion Solver

To verify the accuracy of this pipeline motion solver, we calculate a horizontal placed pipeline (Figure 1) with uniform vertical load on it. The length of the pipeline is 100 m and the diameter is 1 m. The vertical forces are 10 N/m and 30 N/m respectively for two cases. Figure 2 illustrates the comparison between numerical solutions (colored points) and analytical ones. For both cases, our solutions exactly follow the analytical curve. The maximum displacement under 30 N/m is exactly three times of the maximum displacement under 10 N/m, which is reasonable in this linearly simplified case.

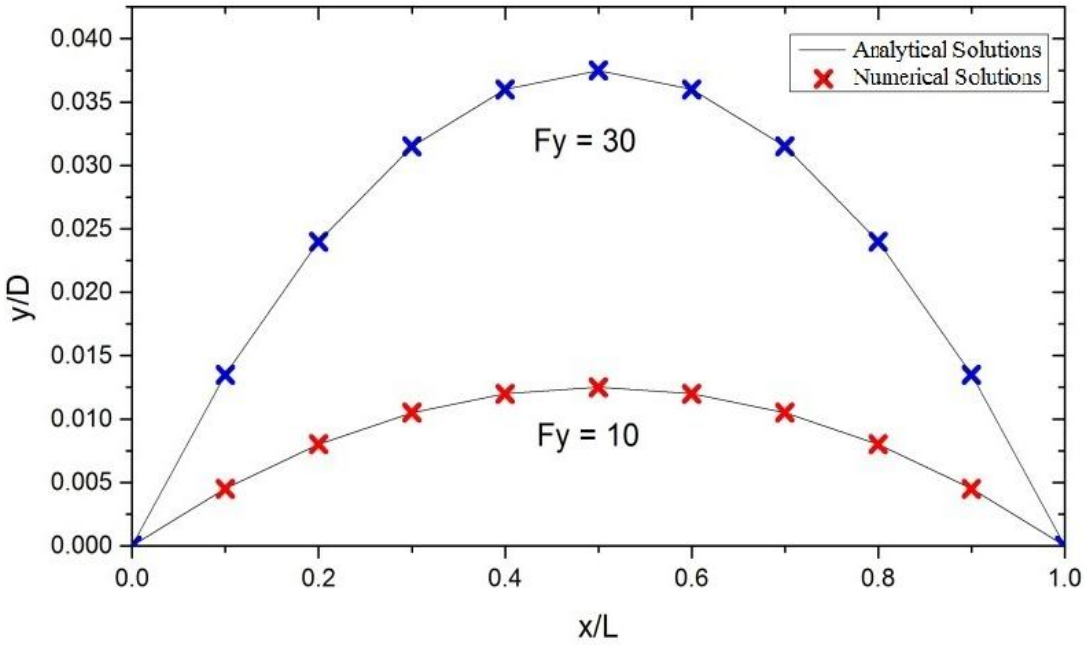

Figure 2 Comparison between Pipeline Motion Solver and Analytical Solutions

Another case is used for justifying the validity of our motion solver in dynamical response. Figure 3 depicts a sketch of this dynamic validation case. A pipeline is horizontally placed with one end fixed on the wall and the other end being left free.

Figure 3 Dynamic Validation Case for Pipeline Motion Solver

We impose a vertically varying harmonic motion at the free end $X(t)=A\times\sin(t)$. A is the amplitude of the motion, and t denotes time variable. For comparison purpose, we

calculate the same case using commercial software OrcaFlex, a package for dynamic analysis of offshore marine systems. The project setup is shown in Figure 4.

Figure 4 Model Test Setup in OcraFlex

A pipeline (yellow) is placed horizontally in the water. The left side boundary condition is set as fixed. Since OrcaFlex doesn't provide a function that can directly define a motion at the end of the pipe, we connect the right side of the pipeline to the center of gravity of a ship (red). By imposing a vertical harmonic motion to the ship, the pipeline will vibrate at the same time.

At a specific length and Young's modulus, the vibration envelope presents pattern as shown in Figure 5, which is calculated by our motion solver. The envelope generated by OcraFlex is shown in Figure 6. The comparison shows a general agreement

between two calculations. The maximum vibration amplitude occurs at x/L=0.2, 0.5 and 0.9 respectively.

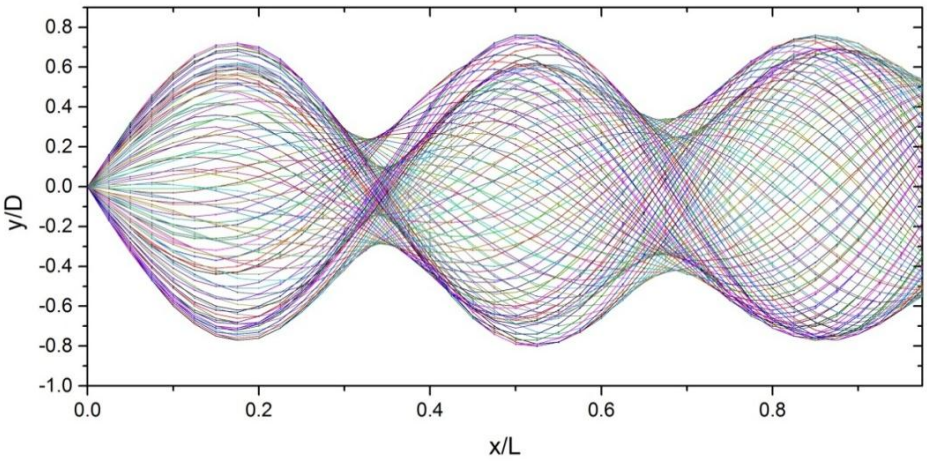

Figure 5 Pipeline Envelope by Numerical Simulation

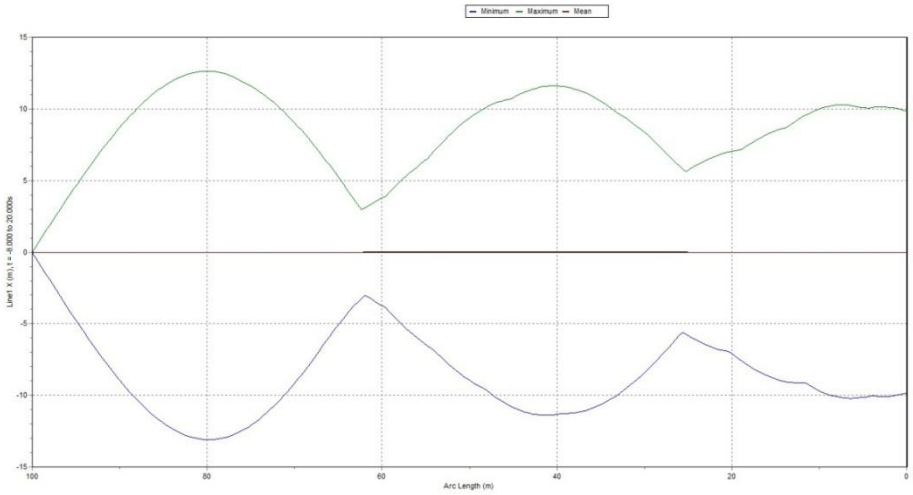

Figure 6 Pipeline Envelope by OcraFlex

Computational Fluid Dynamics Background

The flow field is computed by numerically solving the unsteady, incompressible Reynolds-Averaged Navier-Stokes equations in time domain by means of the Finite-Analytic Navier-Stokes (FANS) code, which is validated in several applications (Chen and Patel, 1988, 1989; Chen et al., 1990, 2013; Pontaza et al., 2004, 2005; Huang et al., 2011, 2012). The turbulence is simulated by a large eddy simulation (LES) model.

An overset grid (Meakin, 1999) is used in this study, for dynamically simulating pipeline motion in a uniform current. When complex geometry existing in a CFD simulation, it is hard to represent the whole fluid domain using a single contiguous grid, even unstructured. In general, different geometrical characteristics can be best described by different types of grid. A suitable approach is to divide the fluid domain into several subdomains and mesh each one with distinctive grid scheme. The subdomains are also referred to as blocks, which have overlapping areas at the interface between every two neighboring blocks. Information of flow field is communicated between adjacent blocks via interpolation at the fringe points, and some grid points may not be used in the simulation, which are called hole points (Petersson, 1999). Generally, overset grid is set up according to the following three steps:

1. Grid generation;
2. Hole cutting
3. Interpolation

In some systems, some of these steps may be combined as one step. A typical overset grid is shown in Figure 7. The red grid is in polar coordinate and the green grid is in Cartesian coordinate. Generally, the grids can be structured, unstructured or a combination of both. The structured-curvilinear gird and Cartesian grid are always employed for simulate complex geometries. When several geometric components occur in a fluid domain, independent body-fitting curvilinear grids will be generated for each object separately, and being embedded into the same Cartesian background grid.

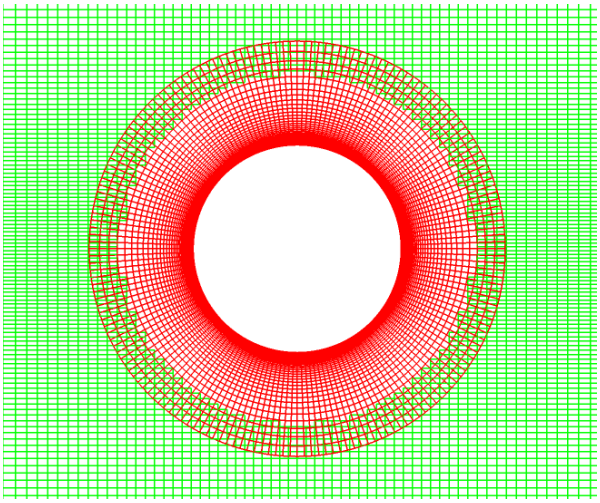

Figure 7 Overset Grid

Hole cutting and interpolation are accomplished by PEGSUS 4.0 (Suhs and Tramel, 1991). The exclusion of points is accomplished by defining a hole creation boundary within the red grid that will define the region within which all green grid points are to be blanked. The points in the green grid surrounding the blanked points are hole boundary points, and they receive flow field information interpolated from grid

points within the red block. Correspondingly, points on the outer boundary of the red grid receive flow field information interpolated from grid points within the green block.

One advantage of using overset grid is that we can manipulate the resolution of a portion of the grid without changing the other parts. In this study, the computational grid is adjusted to very fine resolution near the pipeline outer boundary and sea bottom boundary, whereas the far field grid is relatively coarse.

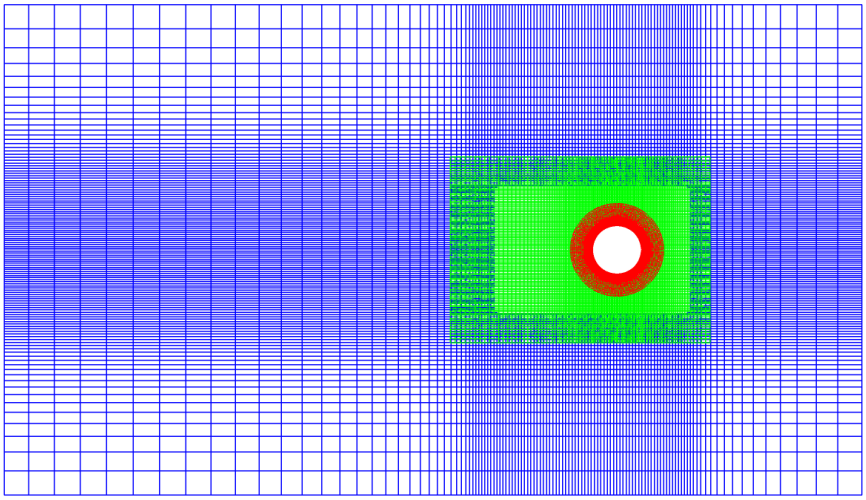

Figure 8 2D Cross Section Grid for VIV Calculation

When dealing with pipeline VIV problem, we generally use three computational blocks to simulate the whole fluid domain: near body grid, wake grid and background grid. A typical cross section of this approach is shown in Figure 8. Near body grid (red) is generated in polar coordinate. The circular area covered by near body grid is the cross section of the pipeline, which is set as wall boundary during the CFD calculation. Wake grid (green) is generated in Cartesian coordinate right surrounding the near body grid. It provides grid that fine enough for vortex shedding and propagation in wake flow area

behind the cylinder. At the interface between near body grid and wake grid, the sizes of the grid from each block are of nearly same magnitude such that the accuracy of communicating the flow field information can be guaranteed. Outside the wake grid is the background grid (blue), which represents the rest area of simulated flow field. Background grid is always of coarse resolution because this is helpful for reducing the total grid points without hurting accuracy. Inside the background grid, there is a rectangular hole cut by wake grid. This follows the same hole cutting and interpolation method mentioned before. The grid scale at the inner boundary of background grid is approximately the same as the grid scale at the outer boundary of wake grid. This again ensures a smooth transition between two computational blocks.

The two-dimensional meshing scheme mentioned above is used for discretizing the flow field at each cross section of the pipeline. Along the pipeline axial direction, we divide the flow field into many parallel layers. In our study, the current is propagating perpendicular to the axial direction in the in-line direction. There is no velocity change along axial direction. Thus, we can approach the spanwise direction with coarse grid.

A dynamic grid scheme is also employed in this approach. As the pipeline moves, near body grid and wake grid will move at the same velocity. This synchronous movement ensures no gap between the pipeline outer boundary and fluid boundary. The background grid will be kept stationary at all times. Another advantage of overset grid is that there is no need to regenerate grid at each time step, which is a time consuming process of CFD calculation. We only need to move the existing blocks and determine the new interface between every two blocks.

Soil Model

Pipe-soil interaction is modeled in accordance with DNV recommended practice for free span pipelines. The soil effect is significant both in the evaluation of the static equilibrium configuration and in the dynamic response of a free span pipeline. The soil is simplified as vertical and horizontal springs with equivalent stiffness and damping. In the in-line direction, the spring model is placed on both sides of the pipeline. In the cross-flow direction, the spring model is placed right below the pipeline. A general approach for vertical and horizontal dynamic stiffness is given as:

$$K_V = \frac{C_V}{1-\nu} \times \left(\frac{2}{3}\frac{\rho_s}{\rho} + \frac{1}{3}\right) \times \sqrt{D} \tag{18}$$

$$K_L = C_L \times (1+\nu) \times \left(\frac{2}{3}\frac{\rho_s}{\rho} + \frac{1}{3}\right) \times \sqrt{D} \tag{19}$$

Where K_V is the vertical dynamic stiffness, K_L is the horizontal dynamic stiffness, C_V and C_L are dynamic stiffness factors which are given in Table 1 and Table 2 for pipe-soil interactions in sand and clay. ν is Poisson's ratio, ρ_s/ρ is the mass ratio of the unit mass of pipeline over the unit mass of displaced water. D is the outer diameter of the pipeline. A medium sand type is selected in this study.

Table 1 Dynamic Stiffness Factor for Pipe-Soil Interaction in Sand (Veritas, 2006)

Sand type	C_V (kN/ $m^{5/2}$)	C_L (kN/ $m^{5/2}$)
Loose	10500	9000
Medium	14500	12500
Dense	21000	18000

Table 2 Dynamic Stiffness Factor for Pipe-Soil Interaction in Clay (Veritas, 2006)

Clay type	C_V (kN/$m^{5/2}$)	C_L (kN/$m^{5/2}$)
Very soft	600	500
Soft	1400	1200
Firm	3000	2600
Stiff	4500	3900
Very stiff	11000	9500
Hard	12000	10500

In general, the axial dynamic soil stiffness is insignificant. However, when dealing with long free spans, an axial soil support model with stiffness should be considered. If there isn't enough information to determine the axial dynamic soil stiffness, it may be chosen as equal to the lateral dynamic soil stiffness as mention above.

Soil damping is also considered in our numerical model. For different types of soil, damping ratio ranges from 0.5% to 4%. The damping ratio differs according to soil

type and the length of pipeline lying on the soil. A value can be selected from Table 3 and Table 4.

Table 3 Modal Soil Damping Ratios (in %) for Sand (Veritas, 2006)

Sand Type	L/D (In-line direction)			L/D (Cross-flow direction)		
	<40	100	>160	<40	100	>160
Loose	3.0	2.0	1.0	2.0	1.4	0.8
Medium	1.5	1.5	1.5	1.2	1.0	0.8
Dense	1.5	1.5	1.5	1.2	1.0	0.8

Table 4 Modal Soil Damping Ratios (in %) for Clay (Veritas, 2006)

Clay Type	L/D (In-line direction)			L/D (Cross-flow direction)		
	<40	100	>160	<40	100	>160
Very soft - Soft	4.0	2.0	1.0	3.0	2.0	1.0
Firm - Stiff	2.0	1.4	0.8	1.2	1.0	0.8
Very stiff - Hard	1.4	1.0	0.6	0.7	0.6	0.5

Fluid-Structure Interaction

In this study, we achieve fluid-structure interaction relying on a partitioned approach: the equations governing the flow and the displacement of the pipeline are solved separately, with two distinct solvers (Bungartz and Schäfer, 2006). The basic procedure of FSI is illustrated in Figure 9. The pipeline motion solver is called by fluid solver as a subroutine. At each time step, we numerically solve the Navier-Stokes equation and obtain the velocity and pressure of the whole flow field. Drag and lift forces are calculated along pipeline surface and read by pipeline motion solver as input. Then, the motion solver computes pipeline velocity and displacement at each computational node and returns the information back to fluid solver for next step calculation. In this way, we achieve the FSI in a partitioned approach.

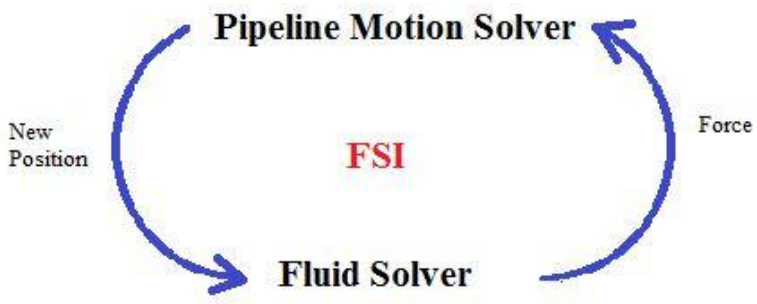

Figure 9 Fluid-Structure Interaction Procedure

For solving fluid domain, boundary conditions and initial conditions need to be specified. The surface of the pipeline is considered as the inner boundary of fluid domain, as shown in Figure 10. The pipeline position and velocity is presented so as to be moving boundary.

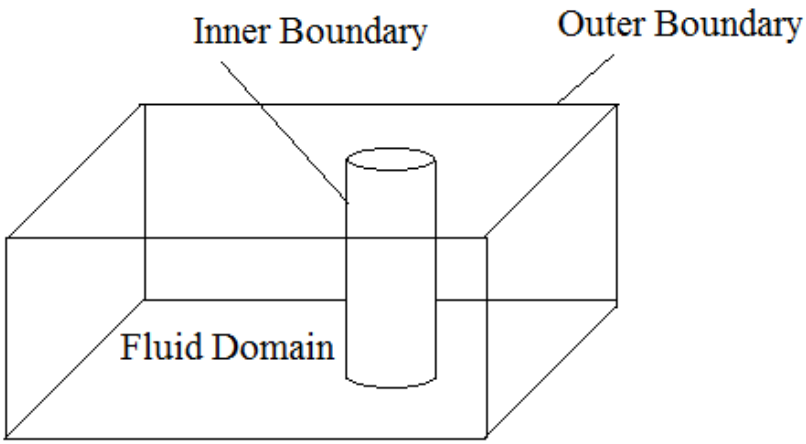

Figure 10 Overview of Fluid Domain

For solving pipeline motion, external force should be calculated. From the results of CFD calculation above, we already have velocity and pressure information. By integrating along the pipeline surface, we can obtain normal and shear forces in both the in-line and cross-flow directions. It is noteworthy that we use relatively coarse grid for fluid domain because we assume the flow field doesn't change severely along the axial direction. In most of our computational cases, 30 layers and 29 segments are enough for smoothly representing axial flow change. However, for pipeline motion solver, we generally divide the pipeline into 200 segments to accurately simulate its movement and profile. Figure 11 shows the mapping relationship between motions solver and fluid solver. When we map the force from fluid solver to the pipeline motion solver, interpolation and extrapolation are needed to acquire force information at every computational node.

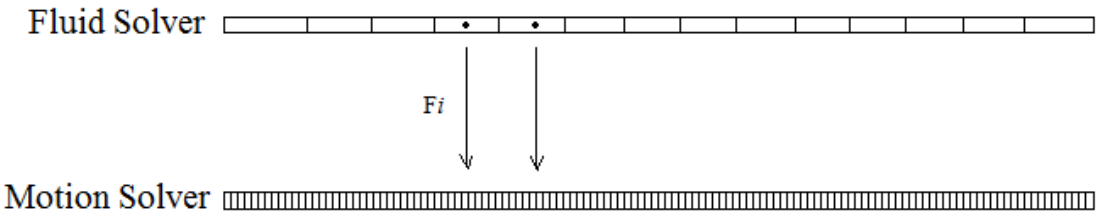

Figure 11 Force Mapping between Fluid Solver and Pipeline Motion Solver

CHAPTER III

VIV SIMULATION OF AN ISOLATED PIPELINE

During the last several years, there are many VIV experiments being conducted and published on deep water slender bodies. MIT Vortex Induced Vibration Data Repository has collected some typical experiments and open to public. Their disseminating of the experimental data is helpful for benchmarking computer codes, developing new theories and gaining insights on what experiments have already been done and what needs to be done next and much more. Especially, the newly released data makes it possible to compare CFD simulation results with model tests in details.

Experiment Background

In this study, we compare our numerical simulation with the experiments conducted by ExxonMobil Upstream Research Company at Norwegian Marine Technology Research Institute. A 9.63 m long pipeline was vertically pinned to the test rig, which would rotate at a constant speed to generate uniform current. The pipeline diameter is 20 mm and thus the aspect ratio is L/D=482, which is considered long span. The other parameters are listed in Table 5 below. Weight in air, pretension and bending stiffness are necessary information for our numerical input.

Table 5 Parameters of an Isolated Pipeline

Parameter	Dimension
Total length between pinned ends	9.63 m
Outer diameter	20 mm
Wall thickness of pipe	0.45 mm
Bending stiffness, EI	135.4 Nm^2
Young modulus for brass, E	1.025×10^{11} N/m^2
Axial stiffness, EA	2.83×10^{6} N
Weight in air (filled with water)	6.857 N/m
Pretension T	817 N

The pipeline natural frequency is another important parameter. We take free decay test to identify the natural frequency of a pipeline with geometric parameters listed above. At the beginning, the pipeline is horizontally placed at its balanced position. At t=0, an impulse load is applied on the pipeline. Then, the pipeline starts to oscillate due to structural stiffness. The amplitude of vibration gradually decreases due to structural damping. Record of the decay history is shown in Figure 12.

To figure out the natural frequency, Fast Fourier transform (FFT) is applied to time domain data. Figure 13 is the result after FFT. The pipeline natural frequency is about 1.9 Hz.

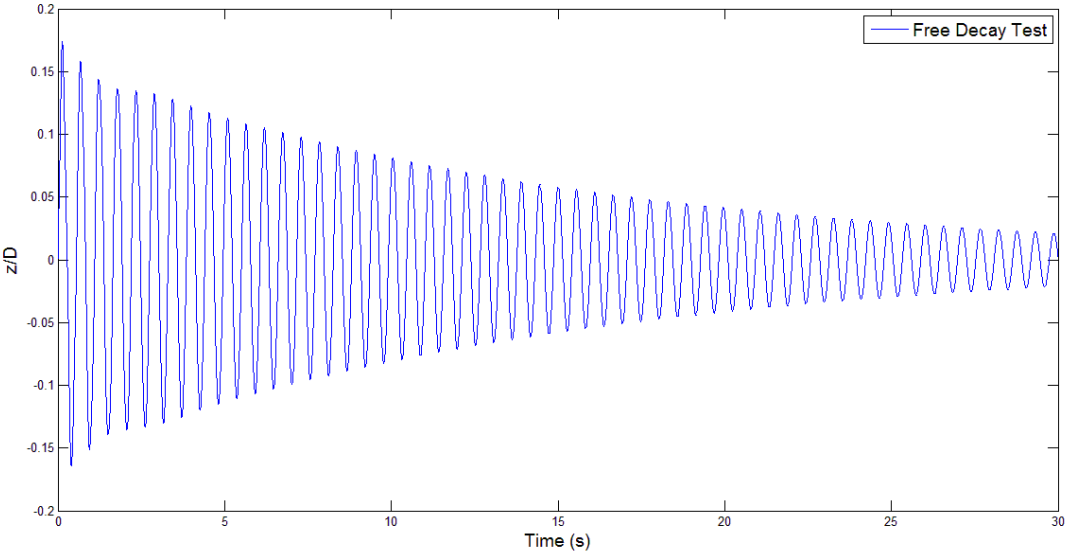

Figure 12 Free Decay Test of Pipeline

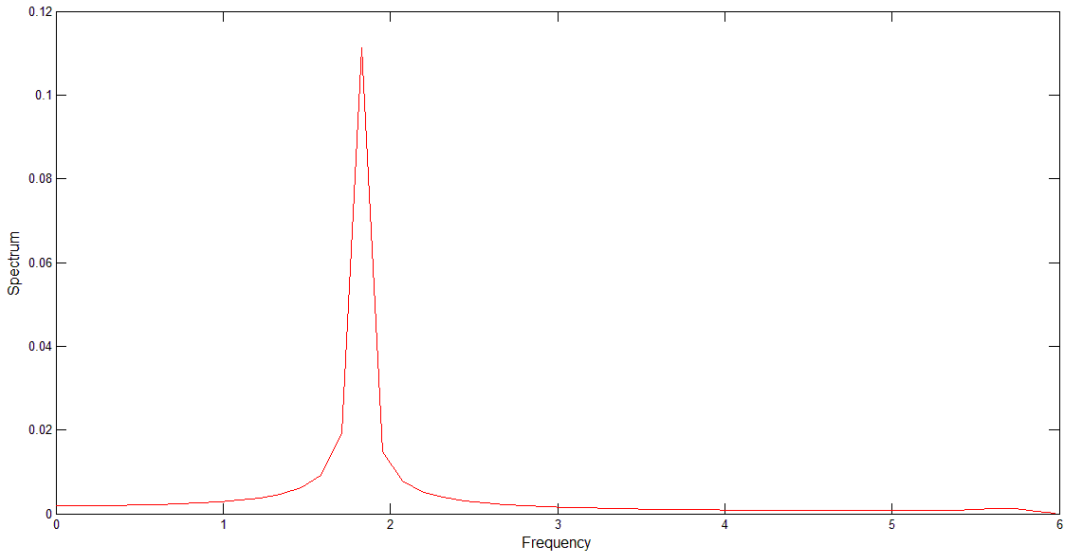

Figure 13 Free Decay Result after Fast Fourier Transform

Grid Generation

The first thing for numerical simulation is generating computational grid. As mentioned before, overset grid scheme is applied for our simulation. For an isolated pipeline placed in infinite fluid domain, we only use two blocks of grid: near body grid and wake grid. Figure 14 is an overview of the fluid domain with a pipeline placed inside. Red block consists 223860 (30×182×41) grid points and green block consists 609030 (30×201×101) grid points. So, there are approximate 0.8 million computational nodes in this simulation. Along the axial direction (X direction in the figure), the fluid domain is divided into 30 layers. In other words, there are 29 elements in the axial direction, with each length of 16.5 diameters ($L_{element}/D=16.5$).

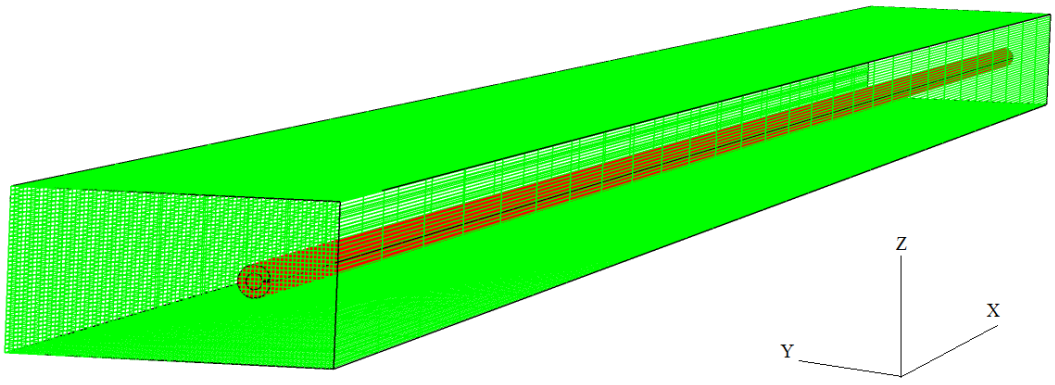

Figure 14 Overview of Fluid Domain for an Isolated Pipeline

A two-dimensional view of the cross section is shown in Figure 15. The pipeline is placed in the middle of the fluid domain. We set the pipeline center at the original

point (y, z) = (0, 0). The flow inlet (right side) is 10D in front of the pipeline, while the flow outlet is 30D behind the pipeline. Both lateral sides are apart from the pipeline center for 10D. The uniform current propagates in the positive Y direction (in-line direction).

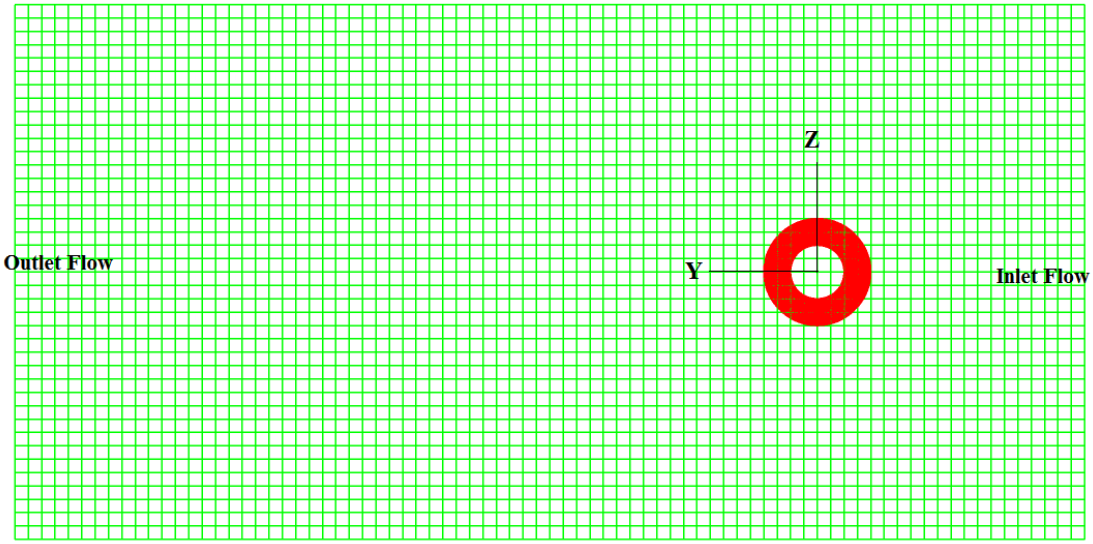

Figure 15 Cross Section of Fluid Domain

A near view of pipeline surrounding grid is illustrated in Figure 16. It is worth mentioning that the red area, which is denoted as near body grid, represents flow field around the pipeline, rather than the pipeline cross section itself. The inner boundary of the read area is the pipeline outer boundary. The near body grid includes 182×41 grid points, with 180 elements in circumferential direction and 40 elements in radial direction. In circumferential direction, 182 grid points create only 180 elements because node #182 coincides with node #2, while node #181 coincides with node #1. By doing

this, the near body grid boundaries (black lines in Figure 17) can read in flow information from the points they are overlapping.

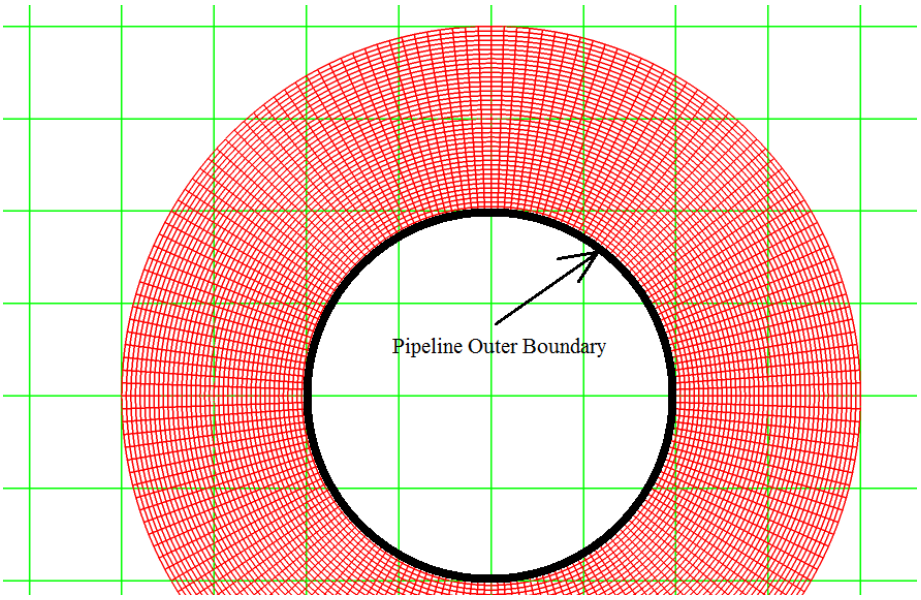

Figure 16 Near Body Grid surrounding the Pipeline

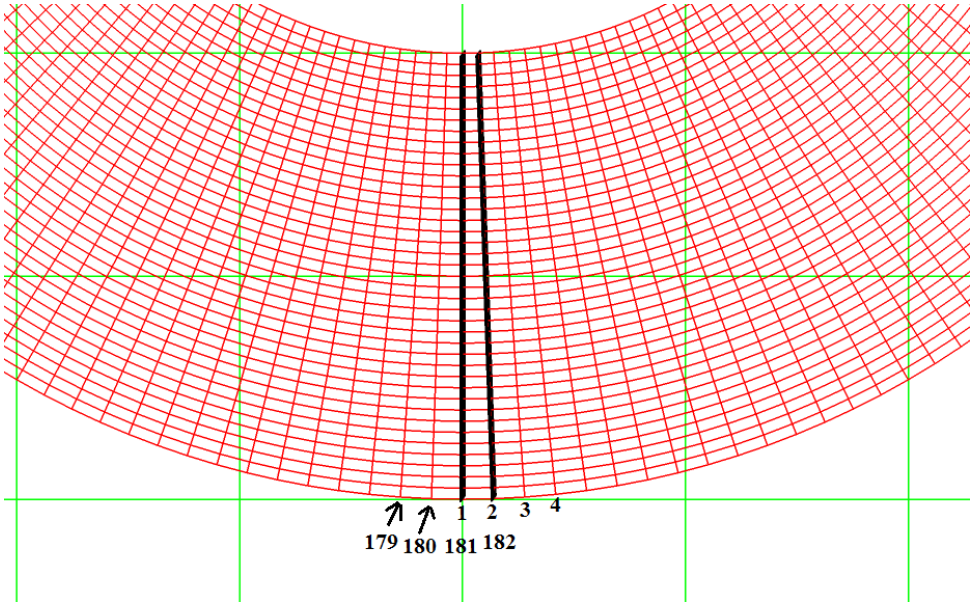

Figure 17 Circumferential Overset Grid

The grid generated above is uniformly distributed over the whole field. However, for pipeline surrounding area, the flow changes dramatically. It requires finer grid to capture subtle changes, especially vortex generation and shedding. Thus, grid refinement is to be carried out. Figure 18 and Figure 19 express the grid after refining. As for near body grid, the size of the innermost element is 0.001D, while the outmost one is of 0.05D. As for wake grid, the closer to the pipeline center, the finer grid we have. The size of wake grid elements ranges from 0.05D to 0.5D.

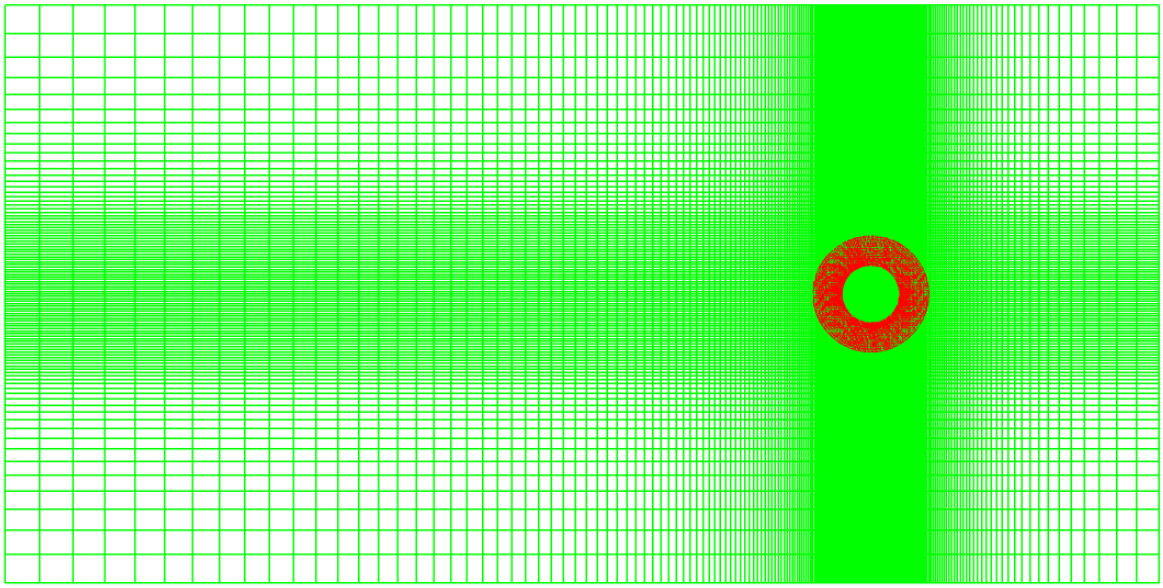

Figure 18 Overview of Grid after Refining

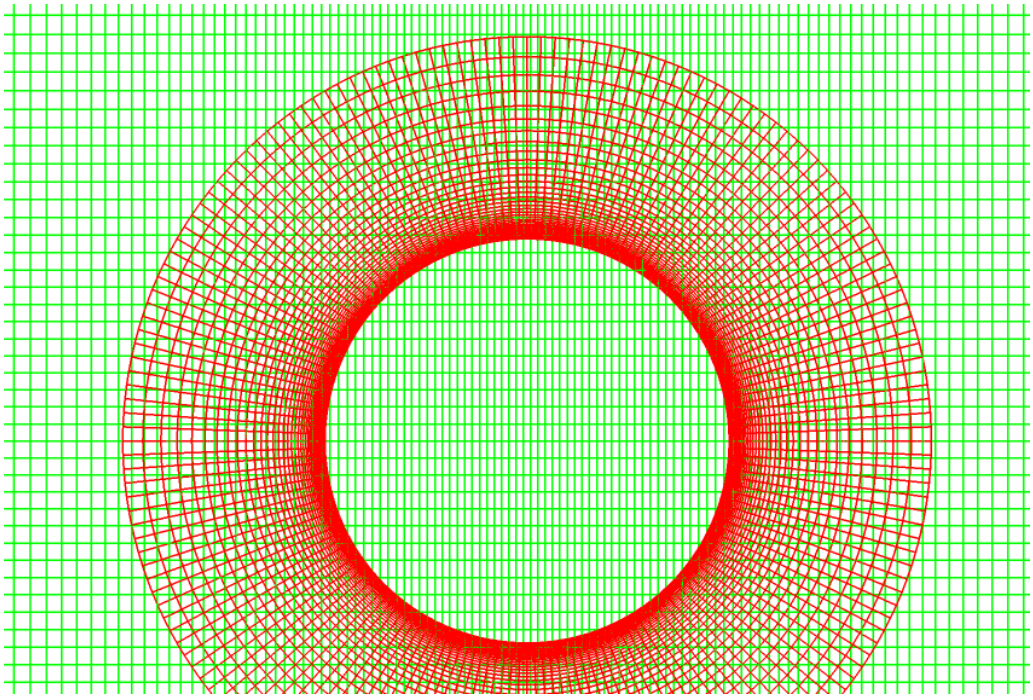

Figure 19 Near View of Grid after Refining

Specifically, we try to make the near body grid size at the outer boundary as close as the size of wake grid nearby. In Figure 20, red and green elements are approximately in the same size. The two blocks communicate with each other according to the following rules: red node 1 locates inside the green element ABCD, such that it receives flow information by interpolating the value of node A, B, C and D. Similarly, green node C can acquire information from red nodes 1, 2, 3 and 4. In this way, the two blocks can exchange any information during simulation. However, if we use grid shown in Figure 21, distortion may happen during the interpolation. There are so many red points in element ABCD that linear interpolation cannot guarantee each point receive true value of flow field information, especially when the flow changes dramatically in this element. Thus, grid structure shown in Figure 21 should be avoided.

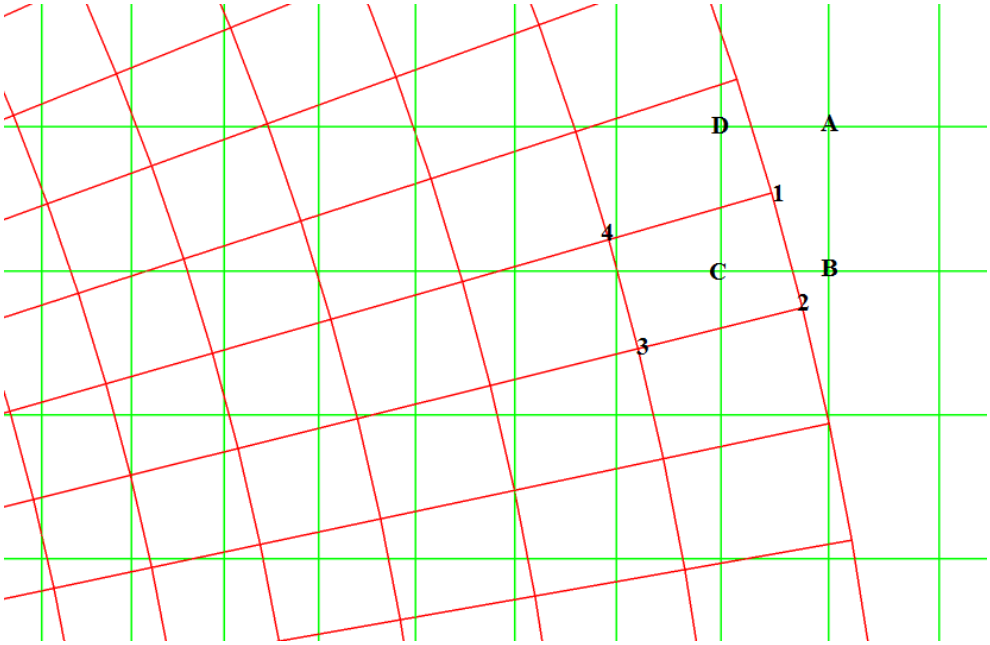

Figure 20 Interpolation between Adjacent Blocks

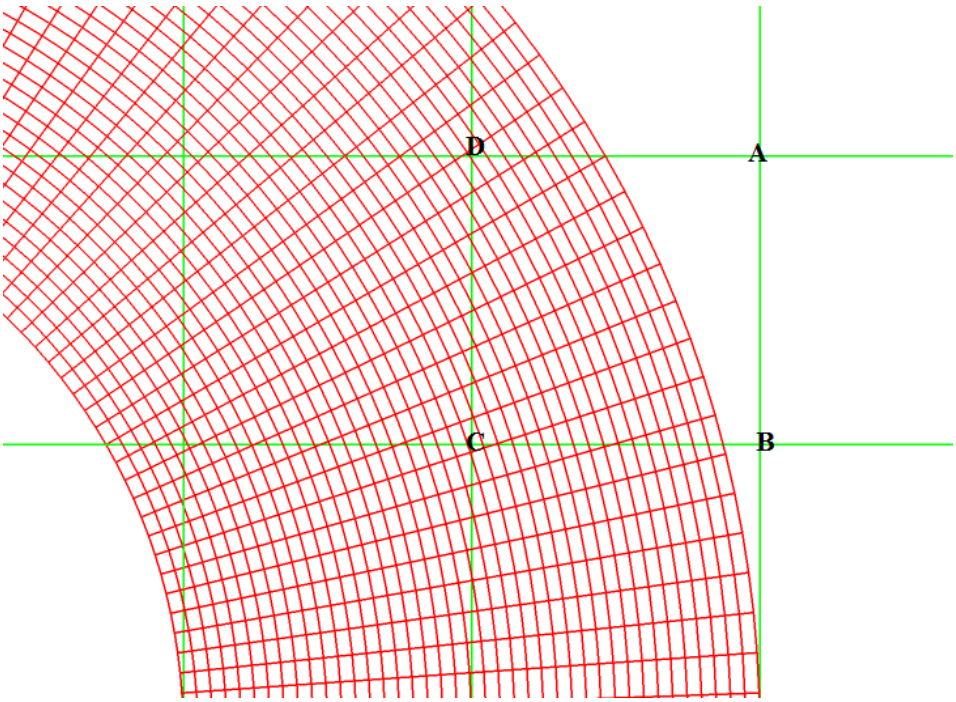

Figure 21 Huge Grid Size Disparity between Adjacent Blocks

The next step is to exclude wake grid points that inside near body grid. In CFD simulation, grid points represent where flow exists. In this study, pipeline occupies the space inside near body grid. Thus, the wake grid should be blanked from that area. We use a circle of near body grid to cut a hole in wake grid. Figure 22 shows the results after cutting. Remaining zigzag green grid forms the inner boundary of the wake grid and will receive information from near body grid.

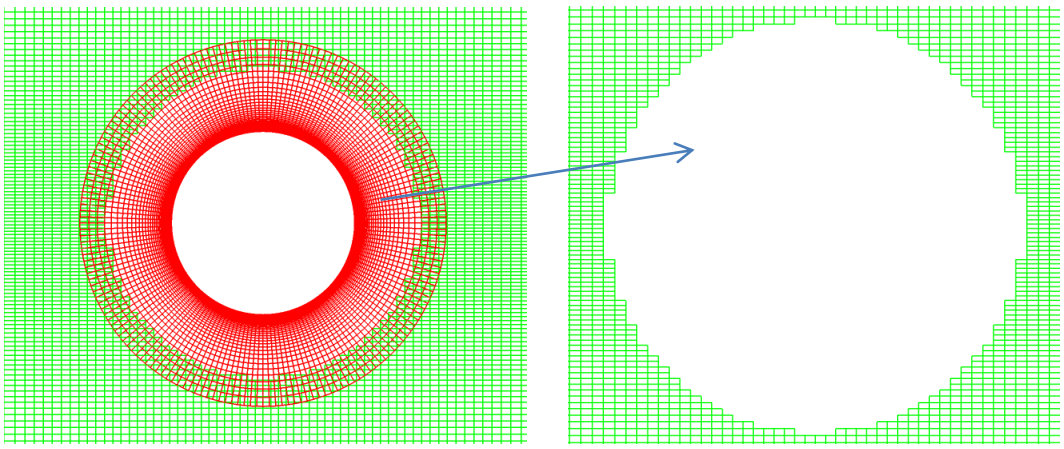

Figure 22 Hole Cutting of Overset Grid

Simulation Results

The pipeline VIV response in a uniform current of 0.42 m/s is analyzed. This is a typical current speed that could occur in real offshore area. At the beginning, the pipeline is straightly placed in still water. When the simulation starts, we gradually increase the velocity of current from zero to target value. As the current passing by, vortex begins to shed from the pipeline surface. Figure 23 illustrate the vortex evolution procedure. Meanwhile, the pipeline begins to deflect towards the in-line direction, as shown in Figure 24. The maximum displacement occurs at the middle section, with amplitude of roughly 2.5D.

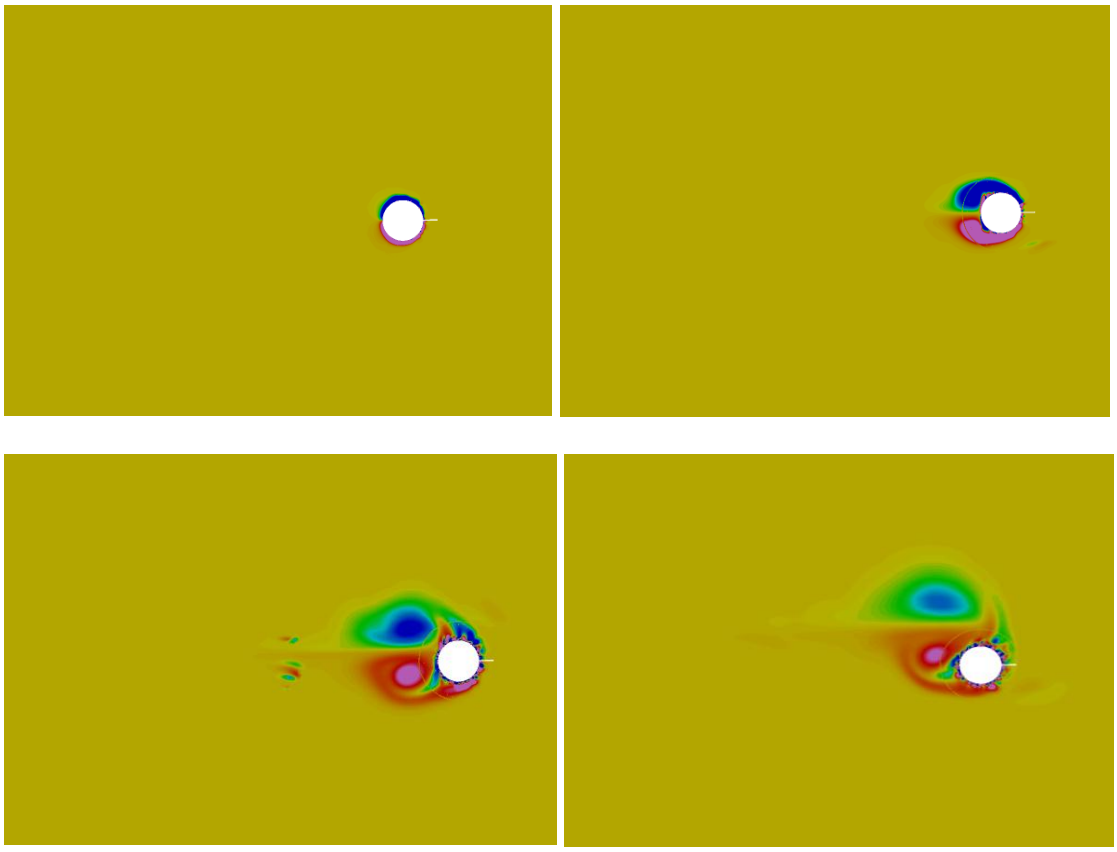

Figure 23 Vortex Evolution in Uniform Current

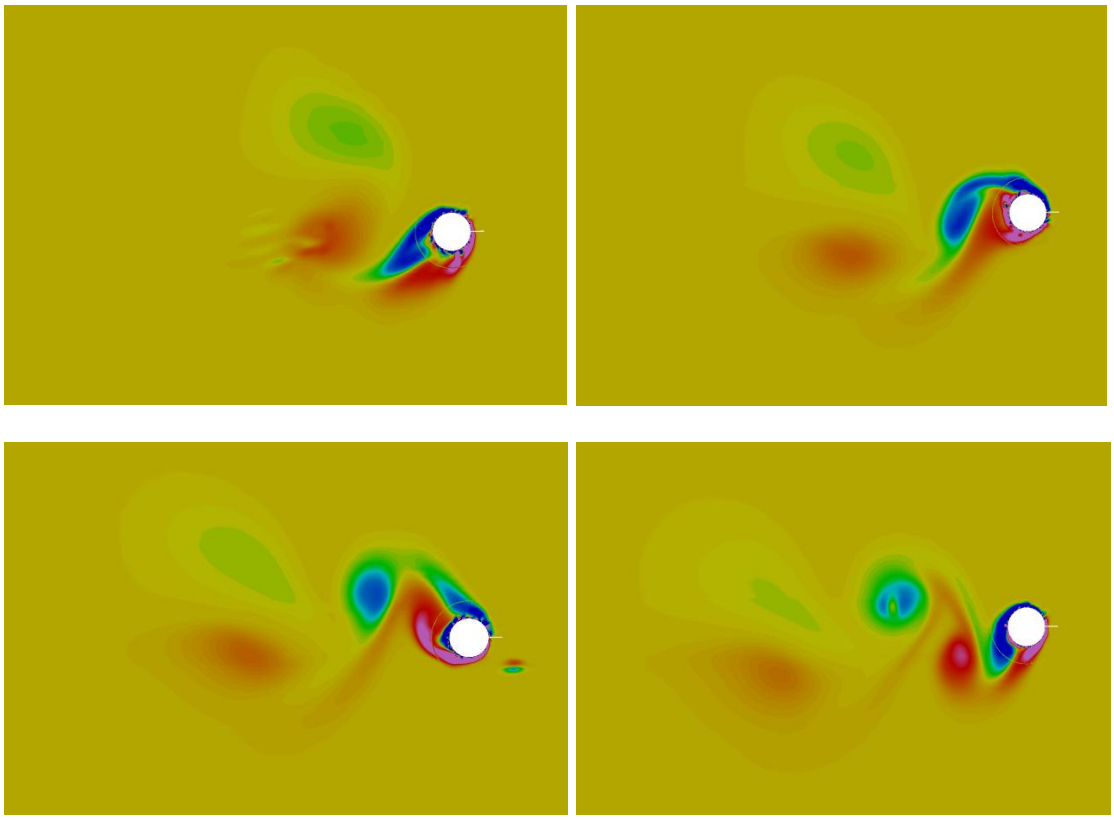

Figure 23 Continued

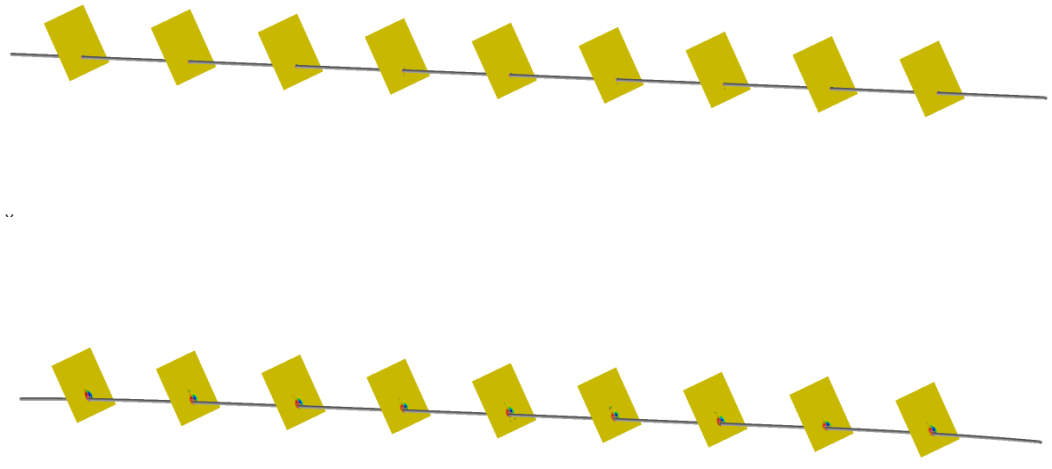

Figure 24 Pipeline Deflection

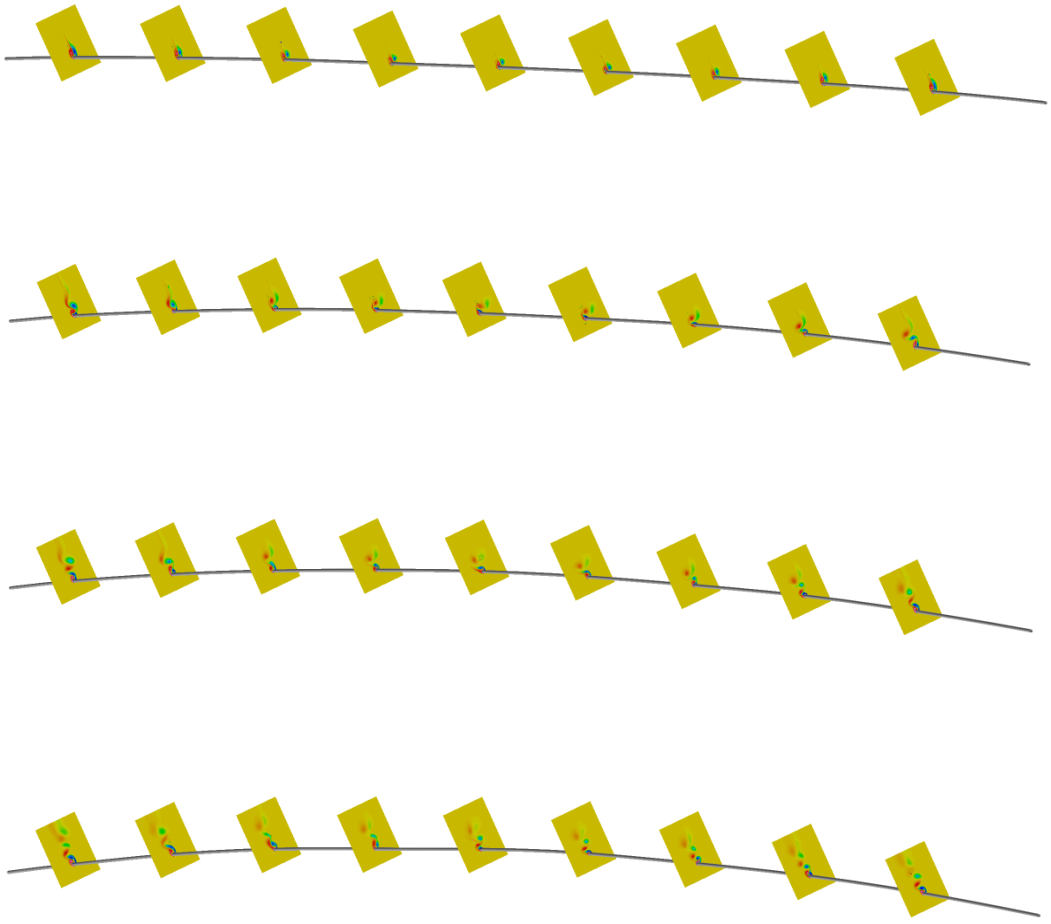

Figure 24 Continued

The pipeline deflection history in the in-line and the cross-flow directions are shown in Figure 25 and Figure 26 separately. We choose the middle section (x/L=0.5) displacement as a representative because the amplitude there is maximum. In Figure 25, as the simulation starts, the pipeline deflects in the in-line direction very quickly. About

0.5s later, the middle section deflection reaches 1.5D. At that time, the pipeline structural restoring force surpasses the fluid force and retrieve the pipeline back to 1.0D over the next 0.5s period. Then, the external fluid force dominates again and lead the pipeline directly to its equilibrium position 2.5D. After 3.0s, the pipeline is stabilized 2.5D apart from its original position and oscillates slightly around its equilibrium point.

In the cross-flow direction, the pipeline begins to vibrate after 1.0s. The average vibration amplitude is about 0.5D. Figure 27 characterizes the process in Y-Z plane. Horizontal axis represents the in-line direction and the vertical axis represents the cross-flow direction. We can see exactly how the pipeline begins to deflect and reaches it stable status. It first goes straightly to 1.5D in the in-line direction with trivial transverse displacement. Then, it turns back and deviates slightly to the negative Z direction. After that, the pipeline travels toward downstream direction immediately, and the transverse vibration becomes significant.

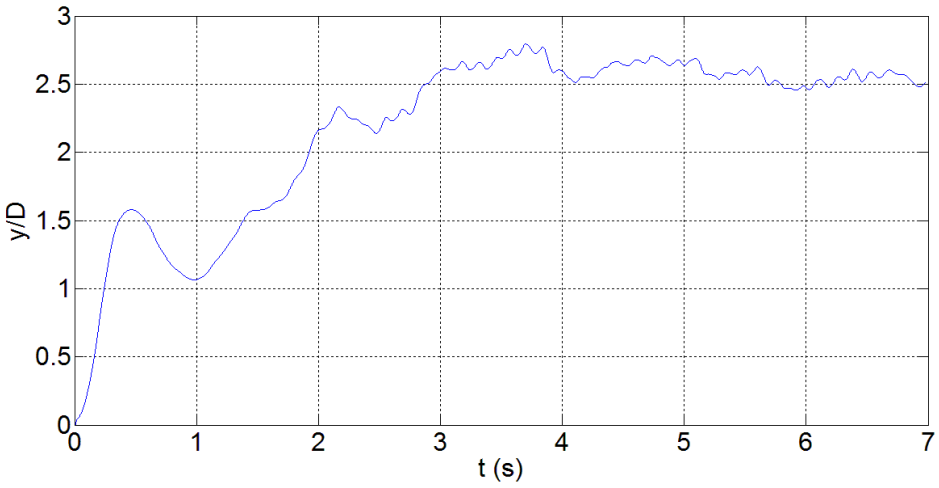

Figure 25 Pipeline In-Line Motion History

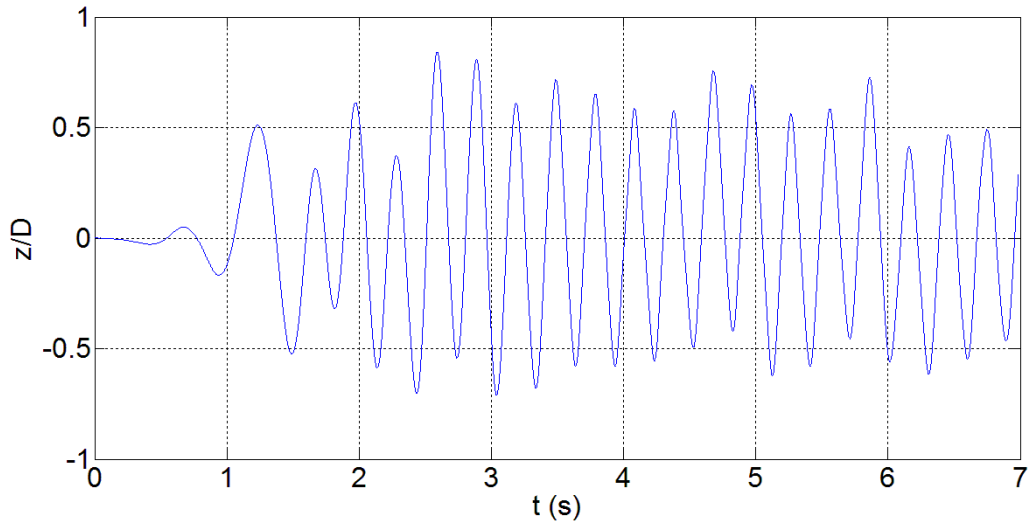

Figure 26 Pipeline Cross-Flow Motion History

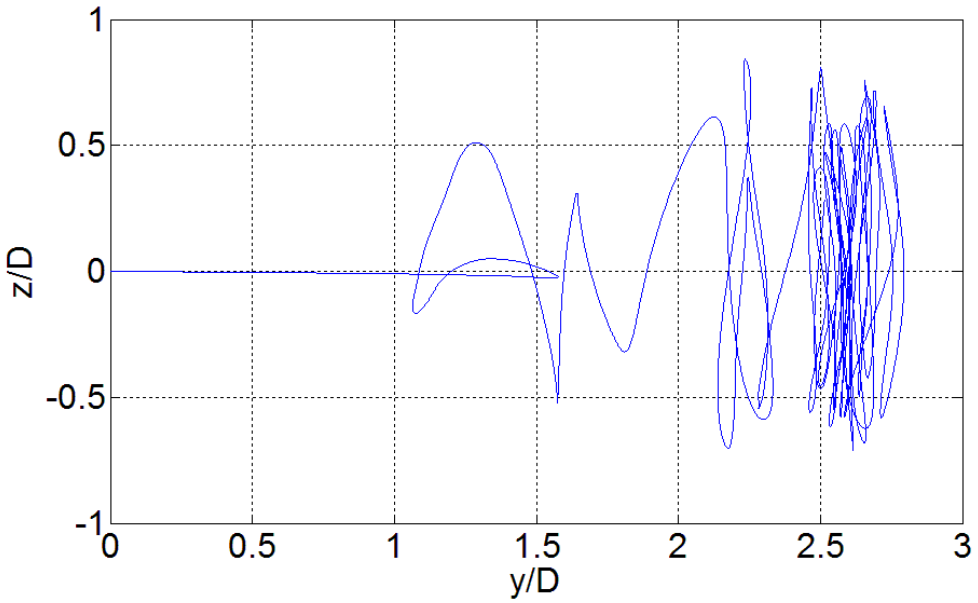

Figure 27 Pipeline Motion History

A comparison is carried out between numerical simulation and experimental results. Figure 28 compares the cross-flow vibration time history. We take a snapshot

from the range 4.2s~7.2s of our numerical simulation. However, the physical model test has a longer starting period. The model test reaches its stable status after several minutes. Thus, we intercept a piece of data from the experiment at stable state and translate it to range 4.2s~7.2s for comparison purpose. In Figure 28, blue line is the experimental result and the red one is the numerical simulation. It can be observed that both amplitudes are of 0.5D magnitude. Also, the vibration frequencies are very close. Figure 29 shows the comparison of the in-line time history. Originally, the in-line vibration of numerical simulation oscillates around 2.5D as mentioned before. In this figure, we translate the plot to Y=0 by subtracting average displacement, again, for comparison purpose. The vibration amplitudes and frequencies are similar. The numerical simulation is not quite stable that there is still noticeable deviation over time.

Normalized vibration amplitude y/D and z/D are compared between numerical simulation and model tests in Y-Z plane. Figure 30 and Figure 31 show pipeline trajectories at stable state. The current propagates from negative-y to positive-y direction. Blue line represents experimental data and the red line represents numerical simulation results. The vibration amplitude is around 0.5D in the cross-flow direction, and 0.2D in the in-line direction. A good agreement can be observed from this comparison. To compare the VIV frequencies, we take Fast Fourier transform (FFT) to convert the data from time domain to frequency domain. Figure 32 shows the results after FFT. The peak frequencies occur at around 2.9 Hz for both cases.

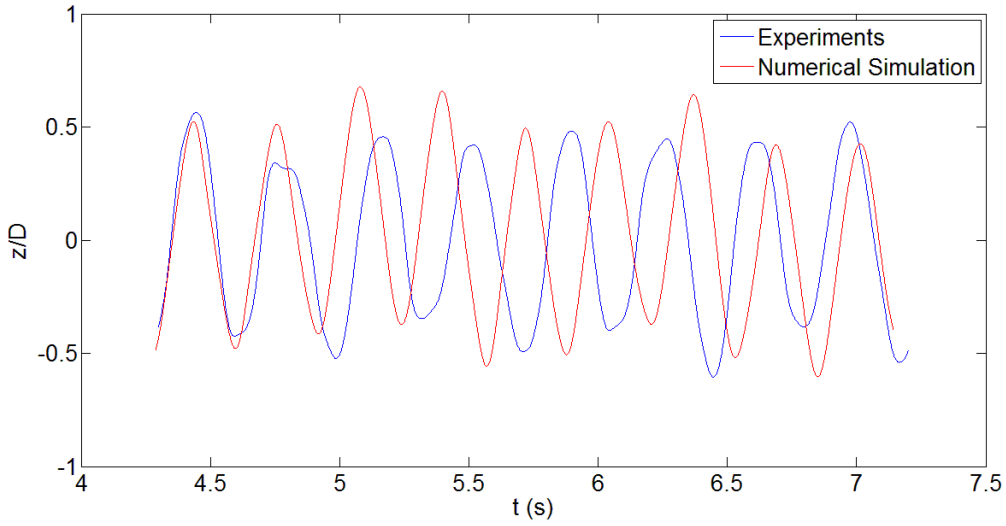

Figure 28 Comparison of Cross-Flow Vibration

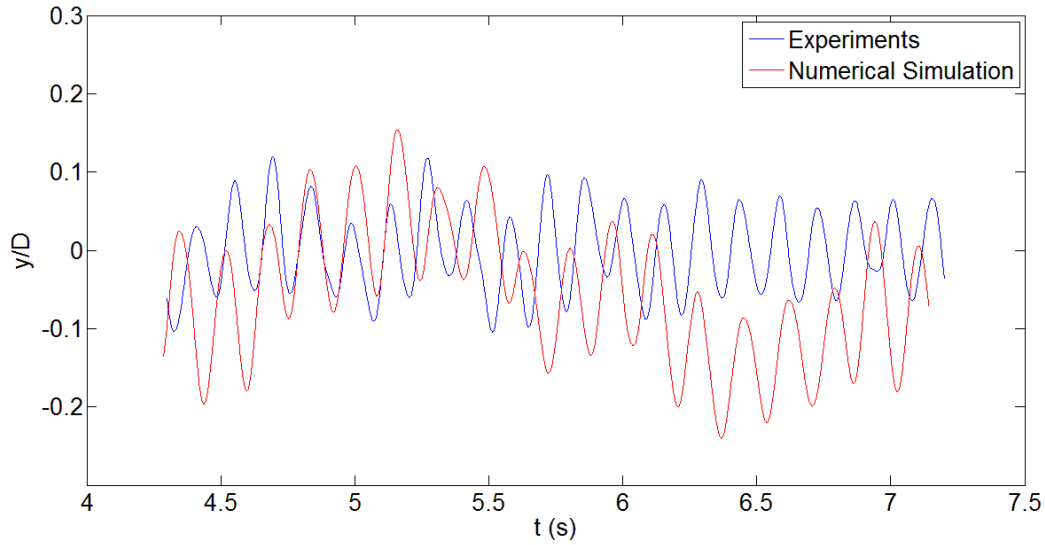

Figure 29 Comparison of In-Line Vibration

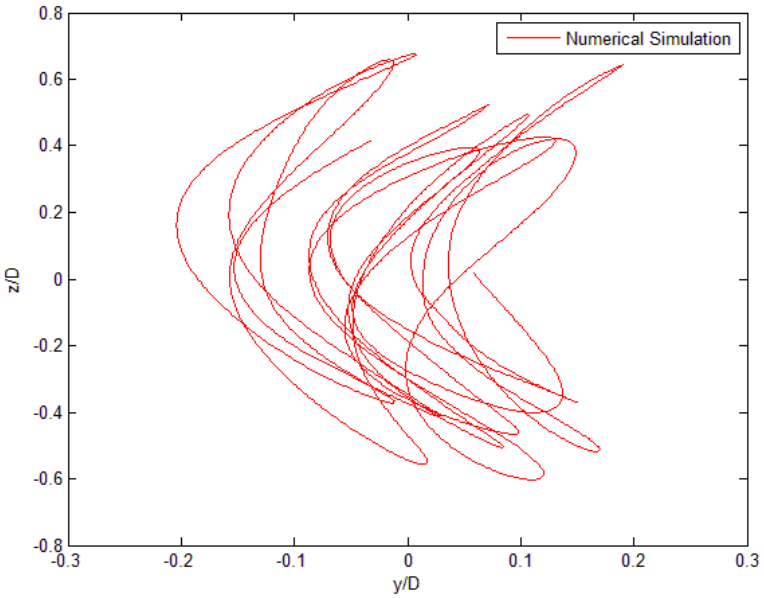

Figure 30 Simulation of Pipeline Trajectory at Stable State

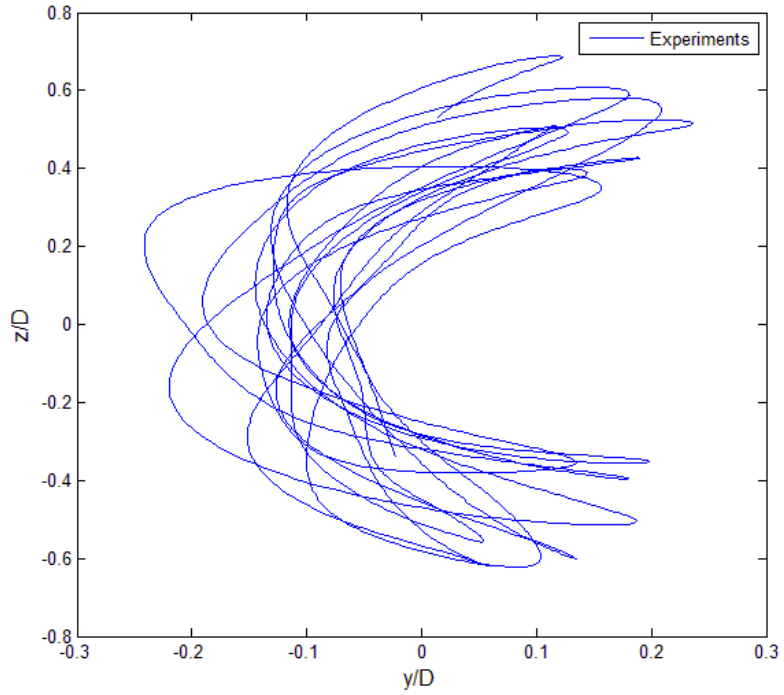

Figure 31 Experimental Results of Pipeline Trajectory at Stable State

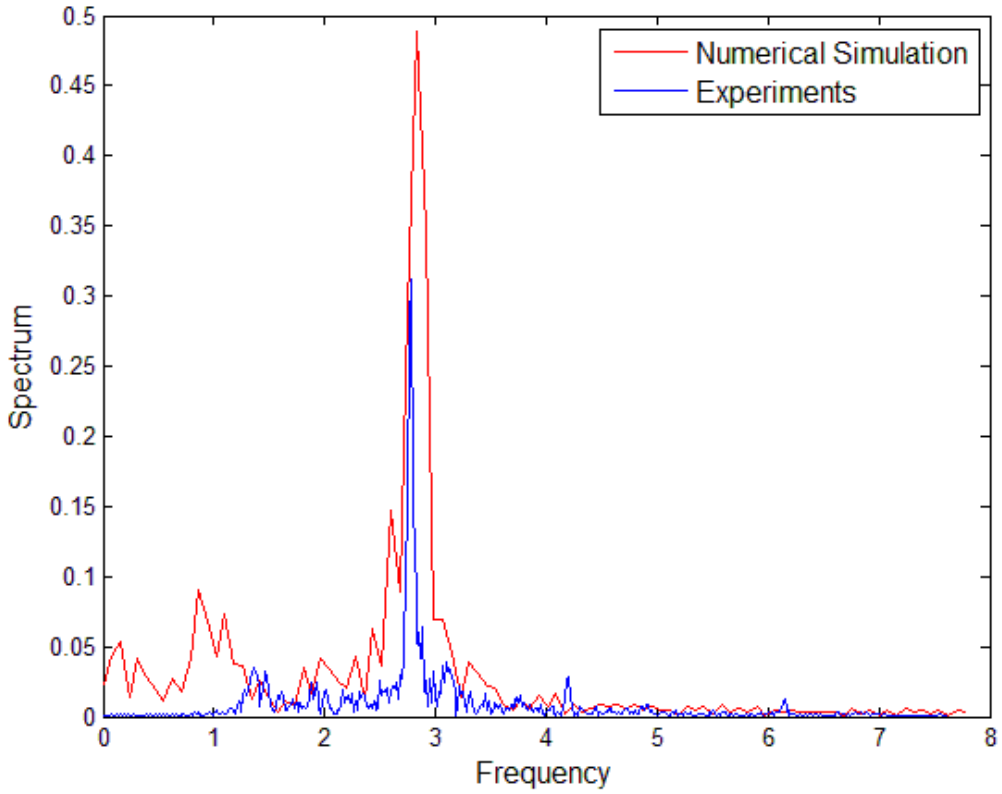

Figure 32 Comparison of VIV Response Frequency

CHAPTER IV

VIV SIMULATION OF A PIPELINE NEAR PLANE BOUNDARY

When a slender body is placed closed to a plane boundary, the VIV response will be quite different from that of an isolated pipeline. The effect of plane boundary proximity on vortex shedding has been experimentally studied by several researchers. The experiments conducted by Bearman and Zdravkovich (1978) revealed that for gap to diameter ratio $G/D>0.3$ the Strouhal number was almost constant. Angrilli et al. (1982) noticed that as the gap to diameter ratio decrease, the vortex shedding frequency would increase correspondingly. Pontaza et al. (2010) observed that in the range of $0.0<G/D<0.3$, there was no classic vortex shedding. The vortex shed from the pipeline was absorbed by the opposite vortex generated by the plane wall. In general, G/D is the key parameter affects vortex shedding of pipeline near wall. In our study, we consider a pipeline of $L/D=150$ parallel arranged close to plane boundary. Gap to diameter ratio ranges from $1.0<G/D<3.0$. The other parameters are listed in Table 6.

Table 6 Parameters of a Pipeline near Plane Boundary

Parameter	Dimension
Total length between pinned ends	1.9 m
Outer diameter	12.7 mm
Bending stiffness, EI	125.0 Nm^2
Weight in air	3.038 N/m
Pretension T	400 N

Grid Generation

Before CFD calculation, computational grid should be prepared for the fluid domain. Again, we use overset grid scheme for the simulation. For a pipeline close to a plane boundary, we use four blocks: near body grid, wake grid, background grid and near wall grid. Figure 33 is an overview of the whole field. Near body grid (red) consists of 223860 (30×182×41) grid points, which is the same as we dealt with isolated pipeline. The wake grid (green) consists of 366630 (30×121×101) grid points. The total number of this wake grid is less than that of the isolated case because we shrink the range of wake grid and add background grid instead to simulate far field flow. Background grid (blue) consists of 316680 (30×116×91) points. A rectangular hole is cut by the wake grid in background grid. In addition, we also have a near wall grid (black) of 88830 (30×141×21) point. Thus, the total grid points are nearly 1 million.

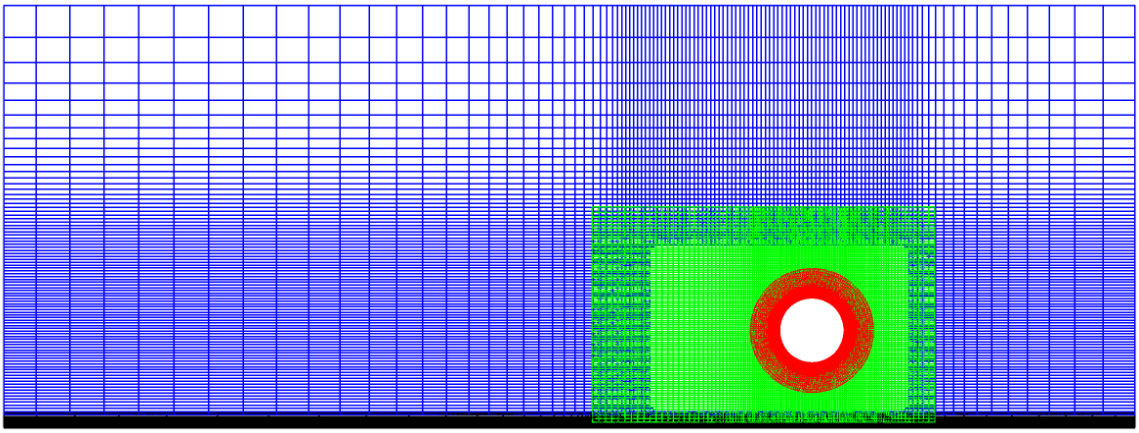

Figure 33 Overview of Grid for Pipeline near a Plane Boundary

A closer view of the near wall grid is shown in Figure 34. For the layer right above the wall, we set the grid size as 0.001D. As it departs from the wall, the grid size

gradually increases and reaches to 0.025D at its upper boundary, which is the same as the size of the background grid at that location. This is for interpolation accuracy consideration as we discussed before.

In this case, we are going to dynamically simulate the pipeline VIV response and its relative motion to the wall. Thus, a dynamic grid scheme is applied. During the whole simulation process, the background grid and the near wall grid will be kept immobile at their original positions. However, the pipeline position should be updated at each time step. Thus, the near body grid and the wake grid will move together with the pipeline at the same speed towards the same direction. Figure 35 illustrates the relative motion of four blocks. The figure on left shows a snapshot of G/D=1.5 and the figure on right shows a snapshot of G/D=0.7. All the grids are kept to their original shape and size. The only difference is that the red block and the green block move downwards and make a new hole in the background grid. A lower limitation is set on the near wall grid boundary that no grid can exceed it. In the right one of Figure 35, part of the green grid points that already exceed the lower boundary have been blanked.

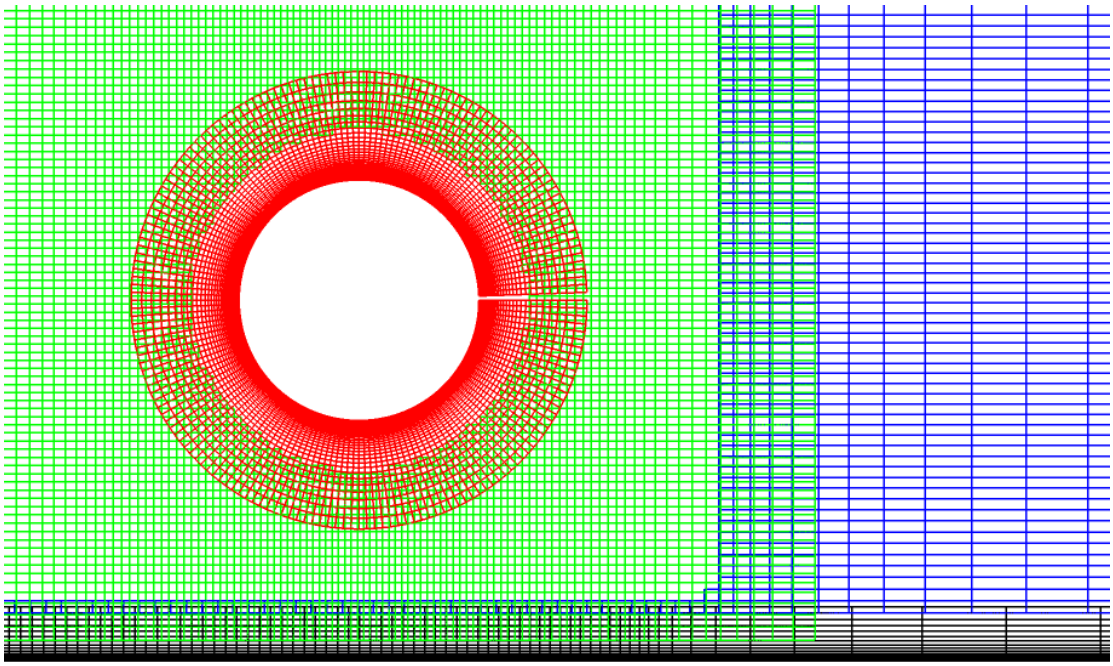

Figure 34 Near view of Pipeline near a Plane Boundary

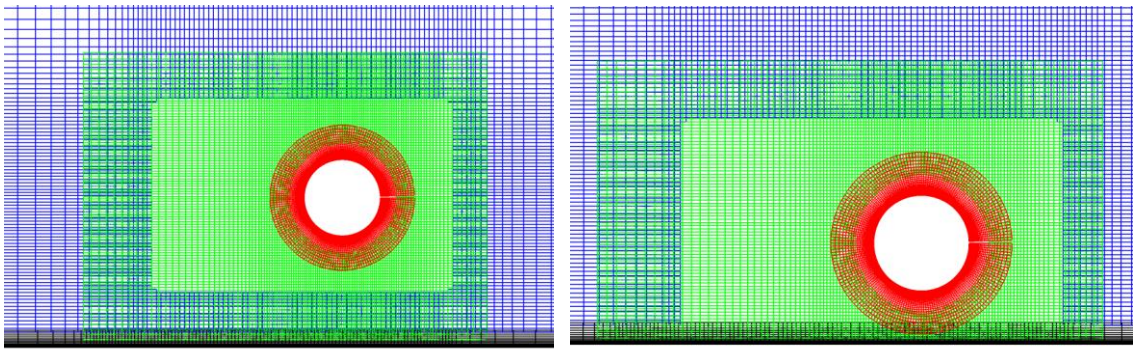

Figure 35 Relative Motion between Computational Blocks

Simulation Results

The pipeline is exposed to sea bottom uniform current of 0.5 m/s. The distance of pipeline to the wall is set to be G/D=1.0, 1.5, 2.0, 3.0 respectively. Figure 36 is the vortex evolving process at G/D=1.0. At the beginning, vortices shed from both sides of the pipeline at the same rate. Then, the vortices develop to 2S pattern and travel toward downstream direction. Meanwhile, the plane boundary also generates vortex in counter-clockwise direction, which cancels the clockwise vortex (pink one) shed from the pipe. In wake flow, the vortices are immediately dissipated and merged into the uniform current. In the in-line direction, the pipeline maximum deflection is 0.5D, as shown in Figure 37, which is very close to its original position.

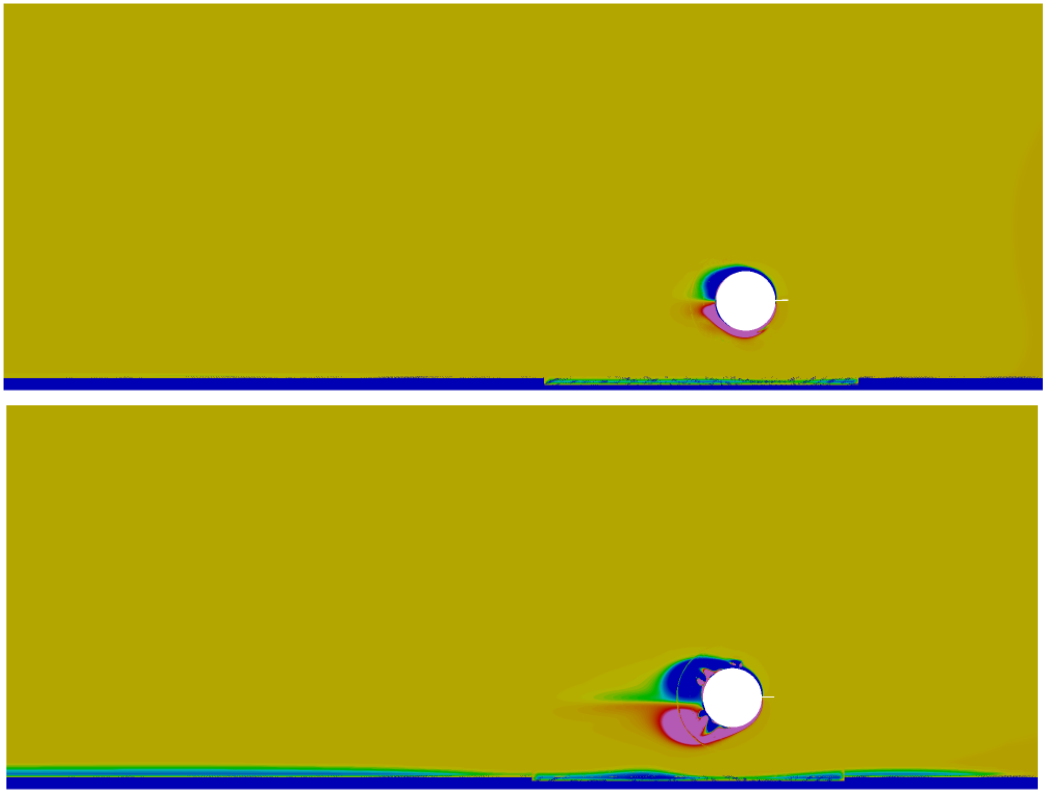

Figure 36 Vortex Evolution of Pipeline near a Plane Boundary

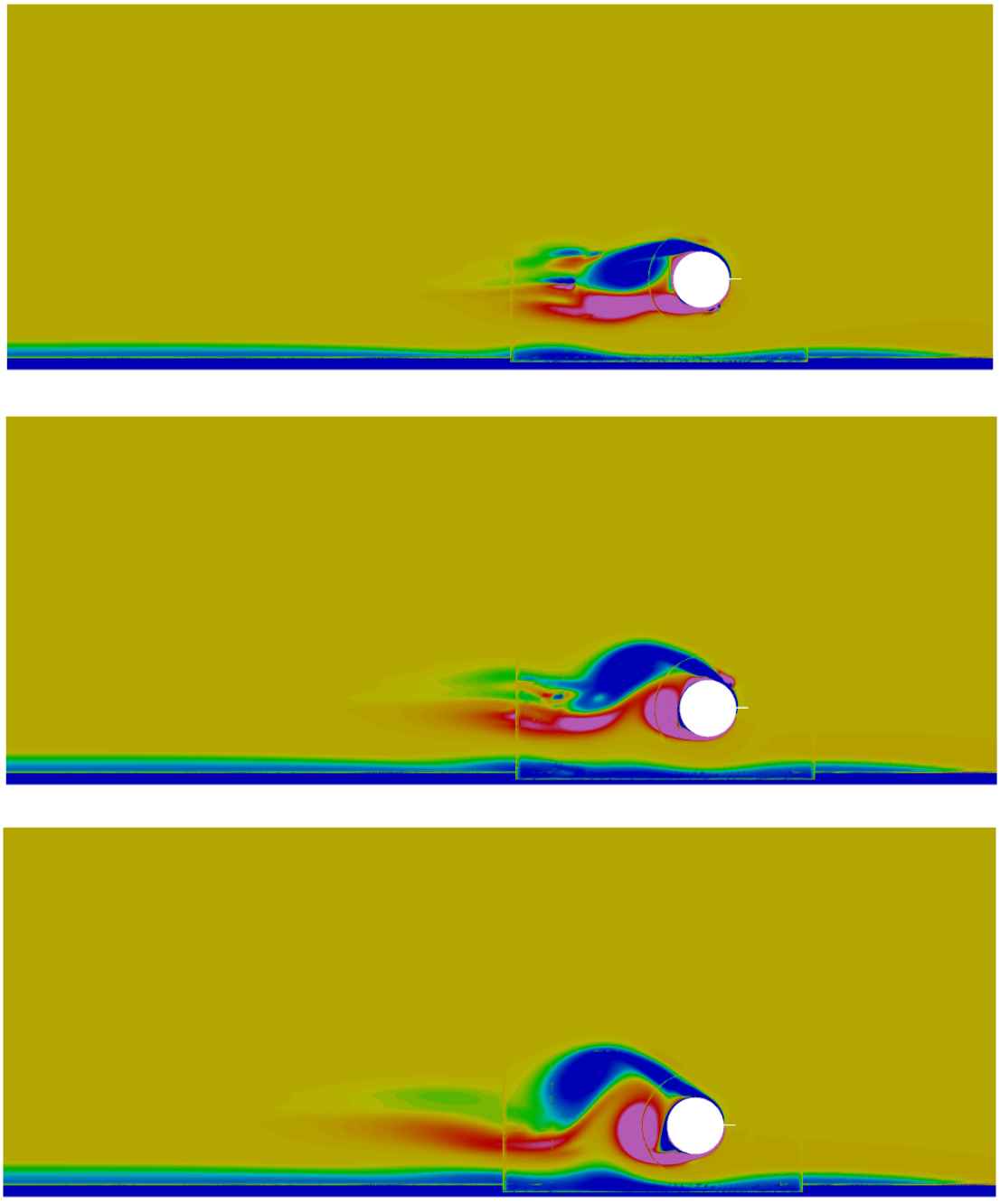

Figure 36 Continued.

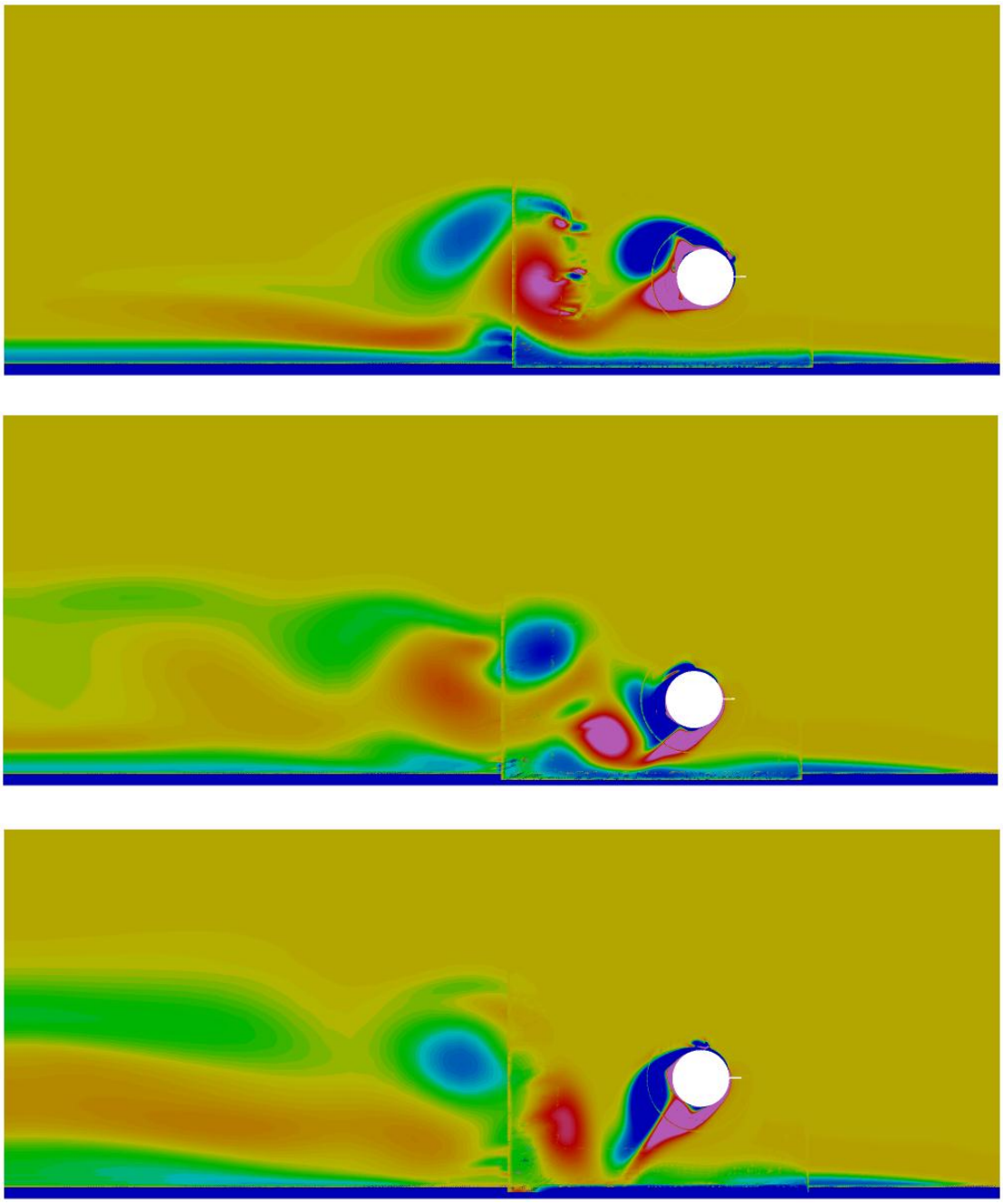

Figure 36 Continued.

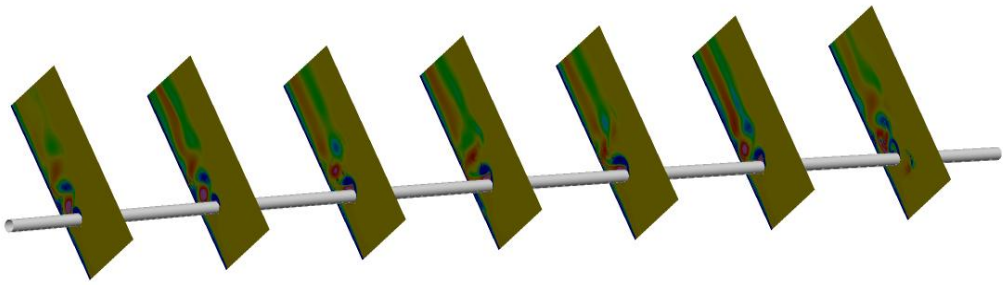

Figure 37 Pipeline Deflection (Maximum Displacement 0.5D)

The time histories of the pipeline cross-flow vibrations are plotted in Figure 38-41. The pipeline starts from static and reaches its steady state after 10s. First, we notice that for smaller gap to diameter ratio, the VIV amplitude is not symmetric about its original position. For G/D=1.0, the positive amplitude is Z=0.84643 and the negative amplitude is Z=-0.7111. This may due the pipeline proximity to the seabed. As the pipeline goes toward seabed, the fluid in the gap would be compressed and becomes a cushion to reduce the pipeline vibration amplitude. For G/D=1.5, the VIV amplitudes are Z=0.80094 and -0.76483 respectively. Even though we can still detect the disparity, but the difference is not as large as that of G/D=1.0. For, G/D=2.0 and G/D=3.0, the positive and negative amplitudes become almost the same, which is as symmetric as the VIV of an isolated pipeline.

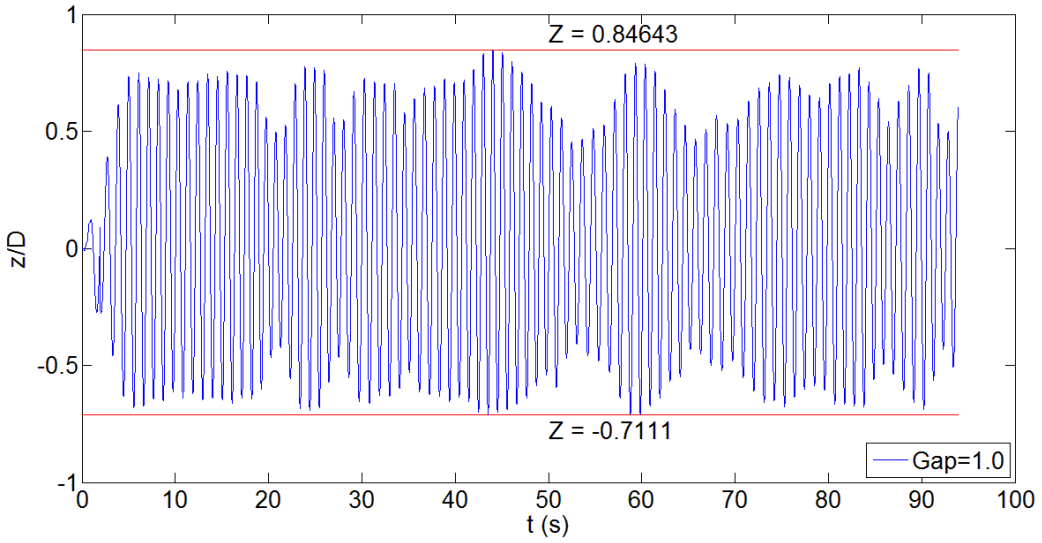

Figure 38 Cross-Flow Vibration History at G/D=1.0

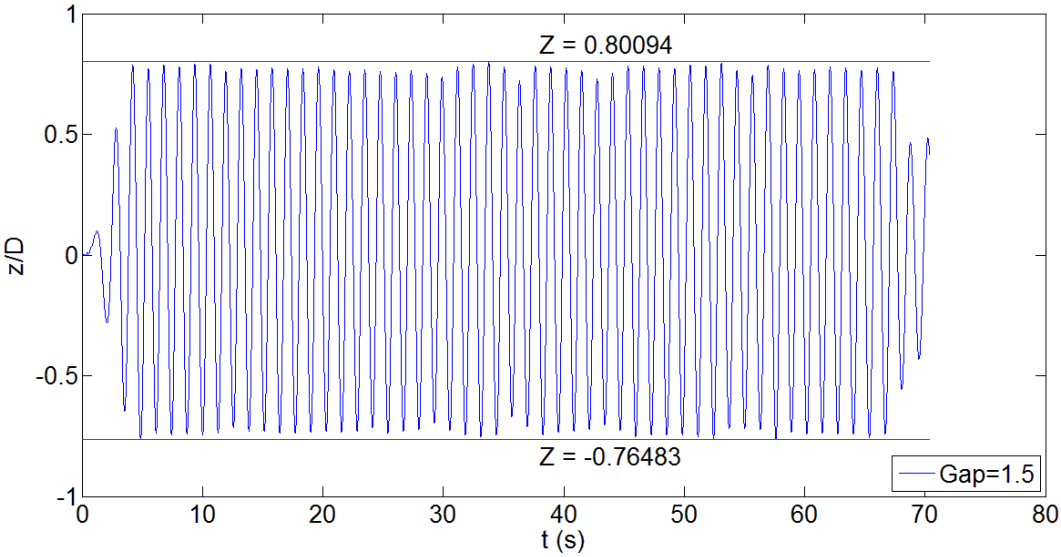

Figure 39 Cross-Flow Vibration History at G/D=1.5

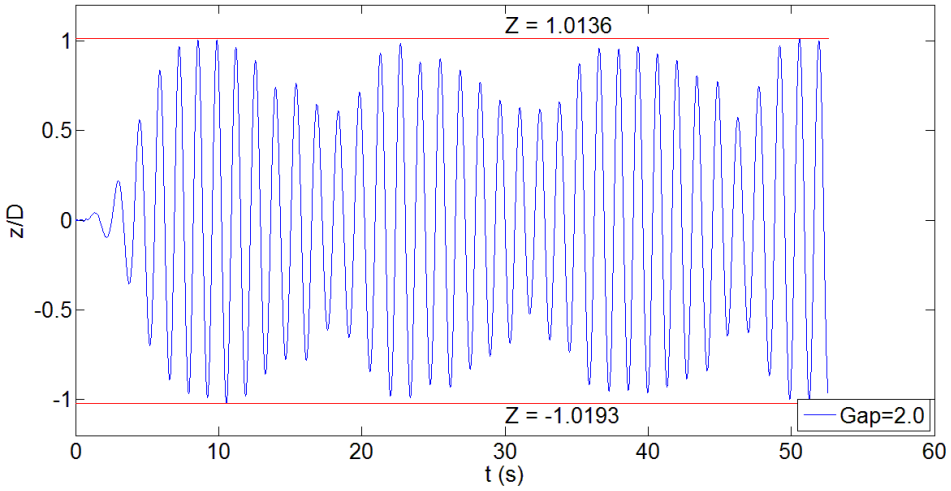

Figure 40 Cross-Flow Vibration History at G/D=2.0

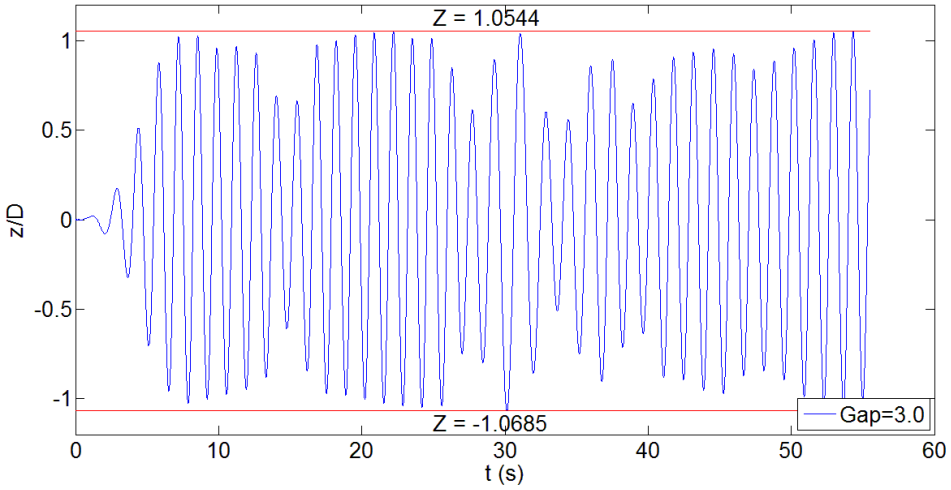

Figure 41 Cross-Flow Vibration History at G/D=3.0

The simulation reveals that as G/D increase, the VIV amplitude will increase as well, which was also proved by some other researchers before (Tsahalis and Jones, 1981). The maximum amplitudes, as we plotted above, don't follow this rule because the maximum values are generated with randomness in every simulation. Thus, we take root

mean square of the whole vibration history to eliminate this randomness. Figure 42 depicts the whole pipeline root mean averaged profile. Figure 43 shows the relationship of averaged amplitudes at middle section of the pipeline versus gap to diameter ratio. Both of them prove that as the G/D increase, the VIV amplitude will increase as well.

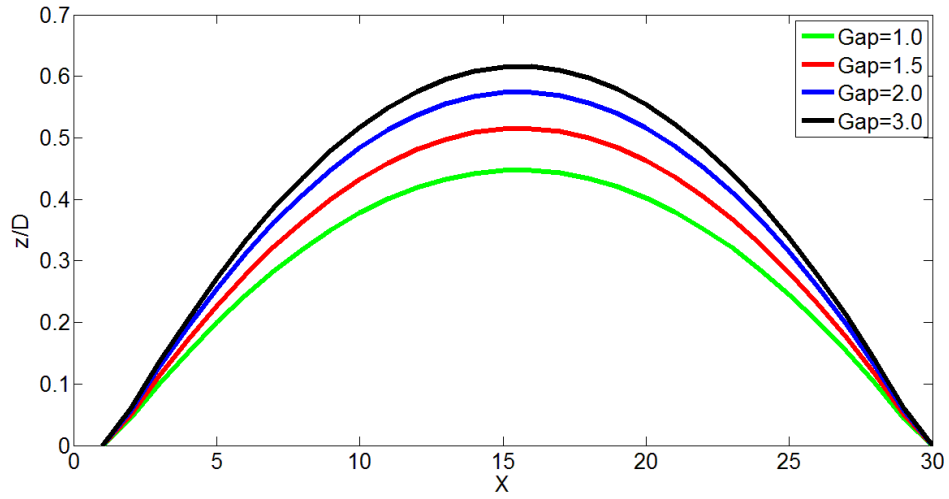

Figure 42 RMS Displacement at Different G/D

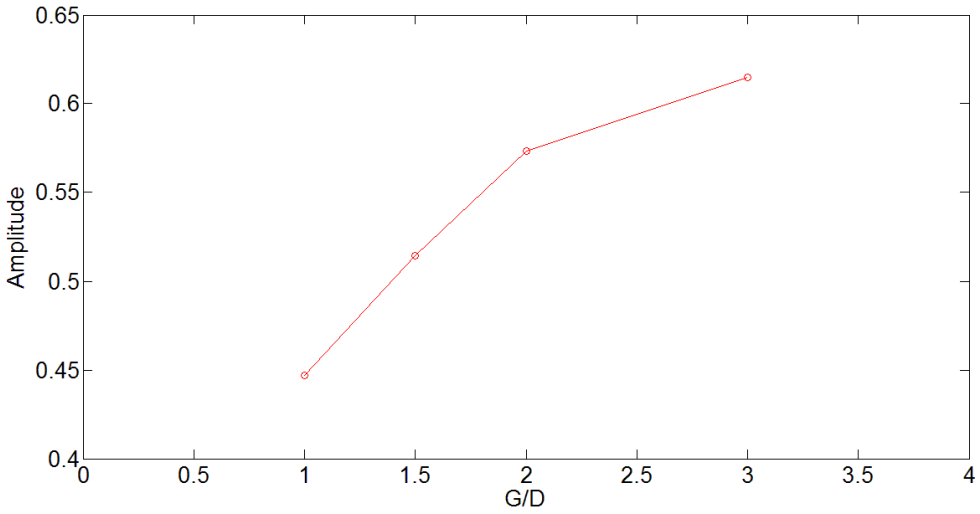

Figure 43 Amplitude versus G/D

In addition, the simulation results shed some light on the relationship between VIV frequency and gap to diameter ratio. Figure 44 shows this relationship. As G/D decrease, the VIV frequency increase significantly.

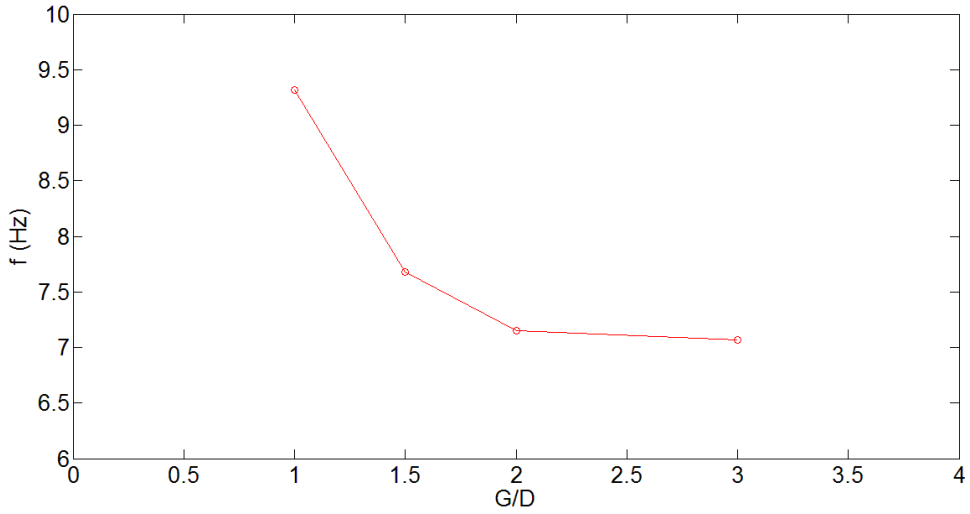

Figure 44 Frequency versus G/D

CHAPTER V

VIV SIMULATION OF A FREE SPAN PIPELINE

Grid Generation

A free span pipeline lying on the soil seabed is depicted in Figure 45. Total length of the pipeline in this simulation is L/D=300, with two ends fixed at point A and point D. Two sides of the pipeline are partially embedded in the soil along segment AB and segment CD. The depth of embedded pipeline is defined as vertical penetration. In this simulation, we set initial vertical penetration as 1/4 of the pipeline diameter. More parameters are listed in Table 7.

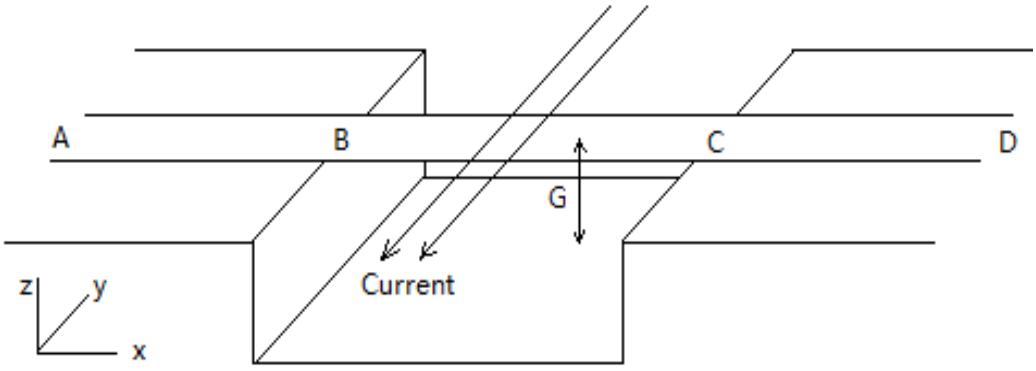

Figure 45 Free Span Pipeline Lying on the Soil Seabed

The middle section is suspended between point B and C. The free span length is half of the total length. A gap-to-diameter ratio G/D=2.0 is chosen in this test. The soil model is also incorporated at the bottom boundary below the gap. So, when the VIV amplitude exceeds the depth of the gap, our FSI solver allows the pipeline to dig into the

bottom and to interact with soil model, rather than hitting on a solid wall. Otherwise, the sudden change of pipeline motion may cause unphysical results. An overview of the whole flow field is shown in Figure 46. In addition to the four computational blocks built before, we add another two blocks: gap grid (yellow) of 41412 (17×116×21) points and wall grid below gap grid (black) of 35955 (17×141×15) points.

Table 7 Parameters of a Free Span Pipeline

Parameter	Dimension
Total length between pinned ends	3.8 m
Outer diameter	12.7 mm
Bending stiffness, EI	130.0 Nm^2
Weight in air	3.038 N/m
Pretension T	500 N

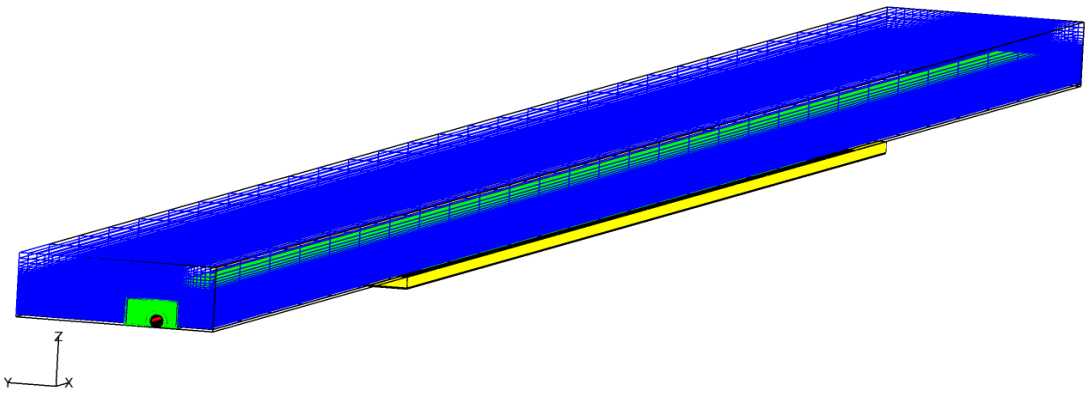

Figure 46 Overview of Flow Field for Free Span Pipeline

A typical cross section is shown in Figure 47. It is almost the same as we used for the pipeline near wall case. The only difference is that we add the gap grid that

serves as part of background flow. For the segments of pipeline embedded in the soil, we need to generate different computational grid. A different scheme is displayed in Figure 48. For this part, we still divide the flow field into four blocks, but all of them have to be cut by the boundary layer between water and soil. As the pipeline moves up and down, the grid around it can be regenerated at each time step. If the pipeline completely moves out of the trench, then, as depicted in Figure 47, a fully covered grid will be generated again surrounding the pipeline.

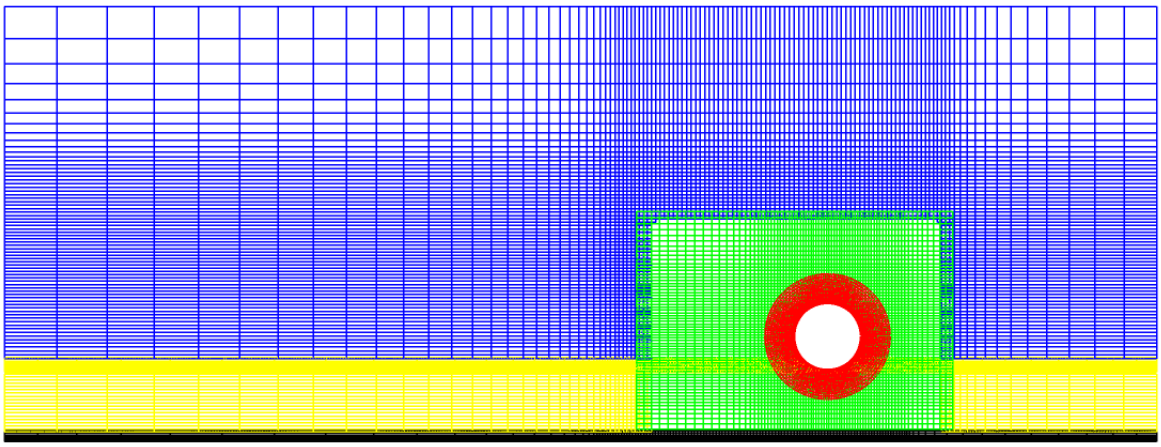

Figure 47 2D View of a Cross Section

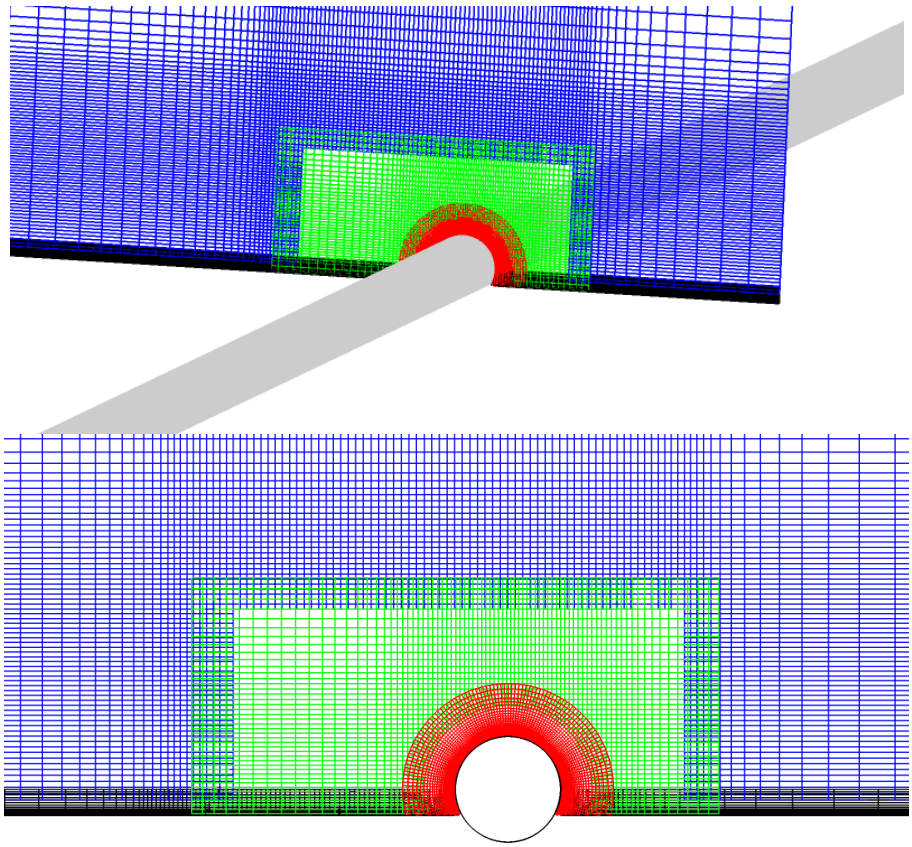

Figure 48 Grid Scheme for Pipeline Embedded in the Soil

Simulation Results

As bottom currents passing by, the pipeline begins to deflect in the in-line direction and vibrate in the cross-flow direction. Figure 49(a) shows the profile of pipeline VIV responses in real dimension. In Figure 49(b), we stretched the cross-flow direction by a scaling factor 30. This figure records the motion history of pipeline VIV. When the pipeline goes downward, two sides are stopped by soil sea bed. When the pipeline goes upward, the whole pipeline will leave the seabed. The in-line displacement is illustrated in Figure 49(c). Maximum displacement is about 0.25D, which occurs at the center of the pipeline.

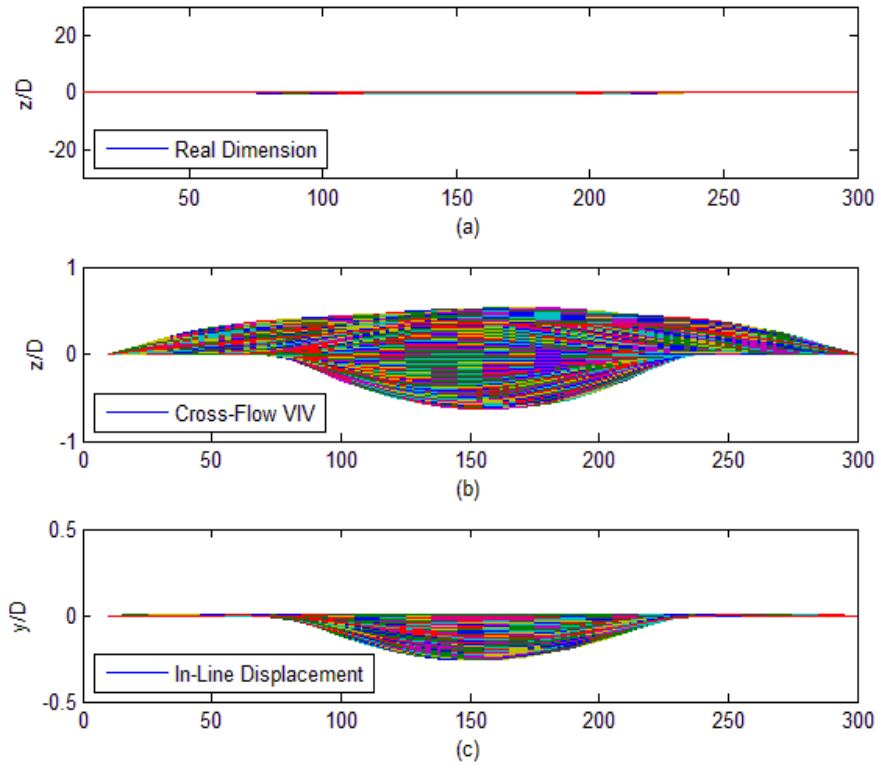

Figure 49 Envelopes of Free Span Pipeline (a) Cross-Flow Envelope in Real Dimension; (b) Amplified Cross-Flow Envelope; (c) Amplified In-Line Envelope

Vortex shedding is visualized in Figure 50. A 2S pattern is again observed in this test. However, unlike the vortex shedding along an isolated pipeline, near bottom vortexes disappear very quickly in the wake flow and mix into bottom current. This vortex energy dissipation may be caused by the friction of bottom boundary.

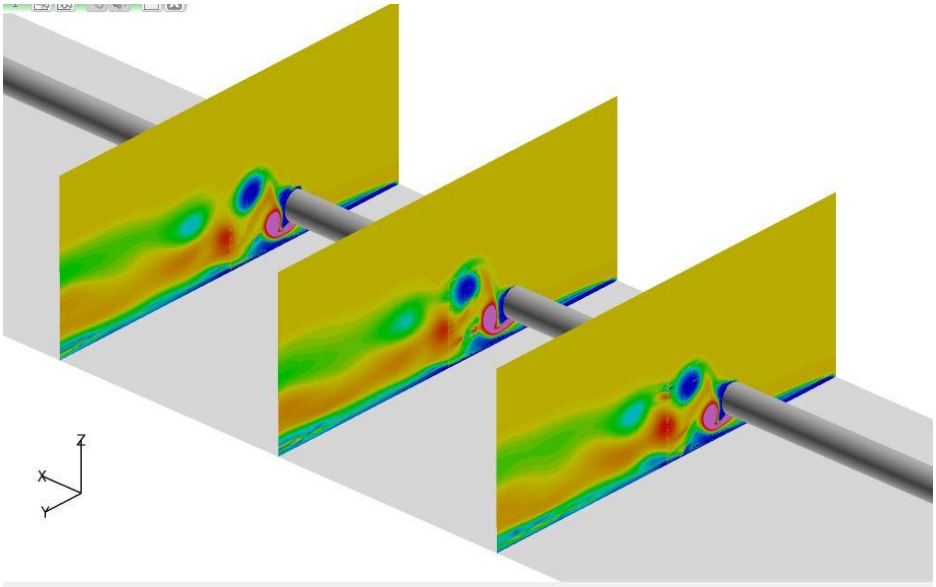

Figure 50 Vortex Shedding of Free Span Pipeline

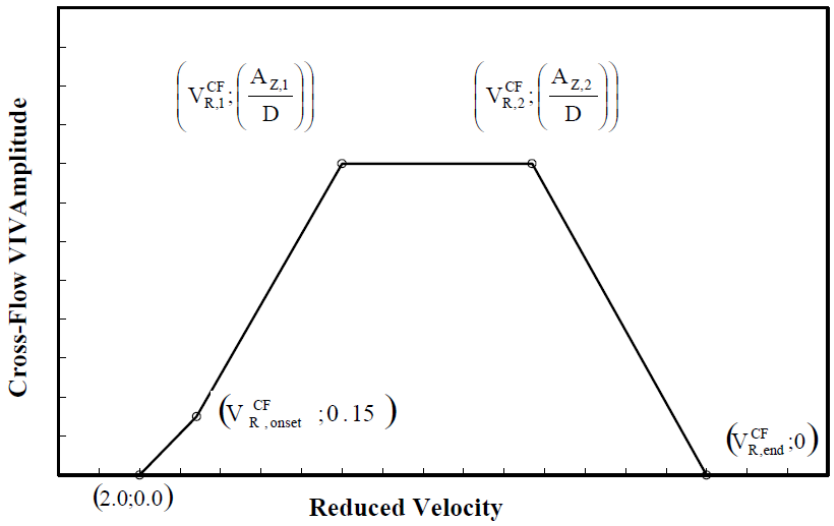

Figure 51 Free Span Pipeline Response Model (Veritas, 2006)

For free span pipeline response, DNV provides two models: response model and force model. The response model is used for free span response dominated by VIV, and the force model is suitable for modeling response under hydrodynamic loads like wave loads. In this study, we only consider the effect of sea bottom uniform currents and neglect waves. Thus, a response model is used for justifying the numerical results here. In Figure 51:

$$V_{R,onset}^{CF} = \frac{3 \times \varphi_{proxi,onset} \times \varphi_{trench,onset}}{\gamma_{on,CF}} \tag{19}$$

$$V_{R,1}^{CF} = 7 - \frac{7 - V_{R,onset}^{CF}}{1.15} \times \left(1.3 - \frac{A_{Z,1}}{D}\right) \tag{20}$$

$$V_{R,2}^{CF} = V_{R,end}^{CF} - \frac{7}{1.3} \times \left(\frac{A_{Z,1}}{D}\right) \tag{21}$$

$$V_{R,end}^{CF} = 16 \tag{22}$$

$$\frac{A_{Z,1}}{D} = \begin{cases} 0.9 & \alpha > 0.8 \quad \left(\frac{f_{n+1,CF}}{f_{n,CF}}\right) < 1.5 \\ 0.9 + 0.5 \times \left(\frac{f_{n+1,CF}}{f_{n,CF}} - 1.5\right) & \alpha > 0.8 \quad 1.5 \leq \left(\frac{f_{n+1,CF}}{f_{n,CF}}\right) \leq 2.3 \\ 1.3 & \alpha > 0.8 \quad \left(\frac{f_{n+1,CF}}{f_{n,CF}}\right) > 2.3 \\ 0.9 & \alpha \leq 0.8 \quad KC > 30 \\ 0.7 + 0.01 \times (\mathrm{KC} - 10) & \alpha \leq 0.8 \quad 10 \leq KC \leq 30 \\ 0.7 & \alpha \leq 0.8 \quad KC < 10 \end{cases} \tag{23}$$

.

$$\frac{A_{Z,1}}{D} = \frac{A_{Z,2}}{D} \tag{24}$$

Here, $V_{R,onset}^{CF}$ is the reduced velocity at which cross-flow VIV of significant amplitude (0.15D) starts. $\varphi_{proxi,onset}$ is a correction factor for seabed proximity, which is chosen as 1 for G/D=2 in this test. $\varphi_{trench,onset}$ accounts for the pipeline location in

trench. In this study, the free span part is out of trench, so $\varphi_{\text{trench,onset}} = 1$. α is the current flow velocity ratio, $\alpha = U_C/(U_C + U_W)$, U_C is the current velocity and U_W is the significant wave induced velocity. In this study, since we neglect the wave effect, $\alpha = 1$. $f_{n+1,CF}/f_{n,CF}$ is the frequency ratio, which is measured as 2.0 in our test. KC is the Keulegan-Carpenter number. Other parameters can be interpreted from Figure 51.

In our test, $V_{R,onset}^{CF} = 3$, $V_{R,1}^{CF} = 6.4$, $V_{R,2}^{CF} = 9.8$, $\frac{A_{Z,1}}{D} = 1.15$. Figure 52 gives the comparison between numerical results and DNV response model for $2<V_R<16$. A general agreement is observed. Also, f/fn versus V_R of numerical simulation in Figure 53 agrees with published experimental studies (Tsahalis and Jones, 1981; Raghavan et al., 2009).

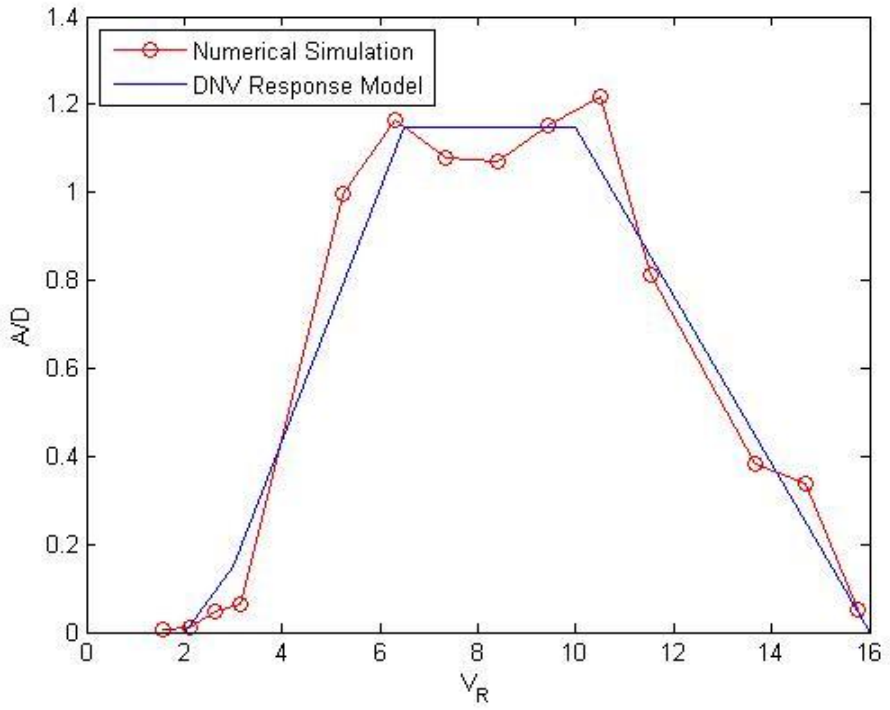

Figure 52 Numerical Simulation Compares with DNV Response Model

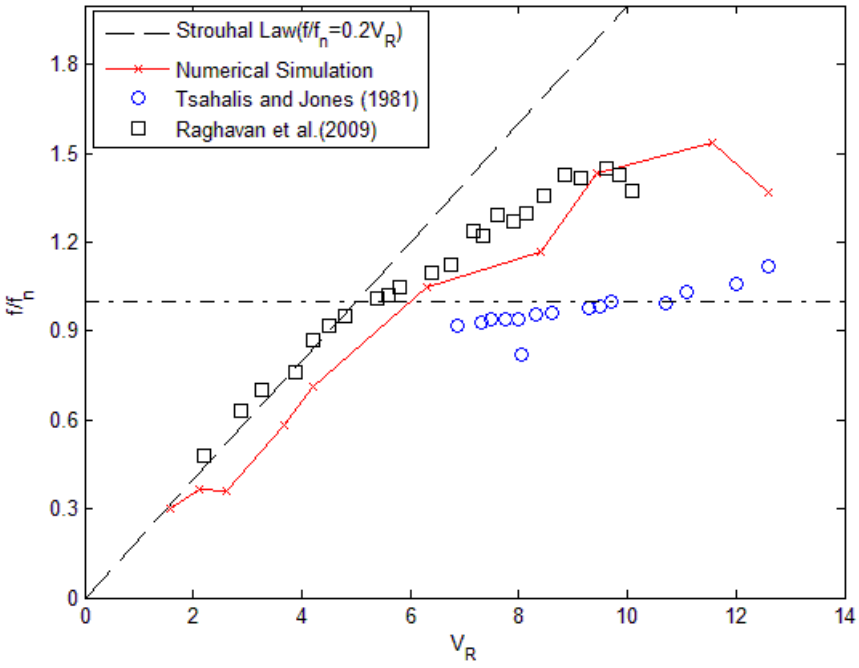

Figure 53 Comparison of f/fn versus V_R

CHAPTER VI

SUMMARY AND CONCLUSIONS

Vortex-induced vibrations of free span pipelines have been investigated in many previous experimental studies, but numerical simulations, especially CFD and FSI, have only been applied recently in this area. In this thesis, we first developed a pipeline motion solver by discretizing tensioned beam equations. Later, we coupled the motion solver with a three-dimensional CFD solver to simulation fluid-structure interactions. A soil model was also included to account for pipe-soil interactions. Overset grid and dynamic grid techniques are incorporated in the CFD approach to facilitate time-domain simulation of arbitrary pipeline motion without the tedious and time-consuming grid regeneration.

First, a static test and a dynamic test were conducted to validate the motion solver. Theoretical solutions and results output by commercial software were used for comparison. A general agreement has been achieved. Then, an isolated pipeline VIV is simulated and compared to experimental data. The simulations show similar responses for a series of tests, including comparisons of pipeline trajectory, VIV amplitude and frequency in both the in-line and the cross-flow directions.

Next, the pipeline VIV near a plane boundary was studied. The influence of the gap to diameter ratio G/D on VIV response has been discussed. In the range of $G/D<3.0$, as G/D increase, the VIV amplitude will also increase, and the vibration frequency will

decrease, which were also observed by other researchers. An asymmetric vibration amplitudes have been detected for pipeline VIV at G/D=1.0 and 1.5.

What's more, the FSI solver was employed for the simulation of a free span pipeline VIV including the effect of pipe-soil interactions. The influence of reduced velocity V_R on VIV amplitude is investigated for $2<V_R<16$ for a free span pipeline lying on soil bed at a gap-to-diameter ratio G/D=2.0. The numerical results match the DNV recommended curve. Also, fitted curve of dimensionless frequency f/f_n is very close to other published experimental data. These results further demonstrated the validity of our FSI solver.

In conclusion, a fully three-dimensional CFD approach for deep water free span pipeline VIV with motion solver and soil model has been presented. The pipeline VIV response is computed in according to the unsteady, incompressible Navier-Stokes equations in conjunction with a large eddy simulation model. The validity and effectiveness were demonstrated by several experimental studies. The numerical simulation results shed some light on the free span pipeline VIV problems.

REFERENCES

Angrilli, F., Bergamaschi, S., & Cossalter, V. (1982). Investigation of wall induced modifications to vortex shedding from a circular cylinder. *Journal of Fluids Engineering*, *104*(4), 518-522.

Bearman, P. W., & Zdravkovich, M. M. (1978). Flow around a circular cylinder near a plane boundary. *Journal of Fluid Mechanics*, *89*(01), 33-47.

Blevins, R. D. (1977). Flow-induced vibration. *New York, Van Nostrand Reinhold Co., 1977. 377 p., 1*.

Bungartz, H. J., & Schäfer, M. (Eds.). (2006). *Fluid-structure interaction: modelling, simulation, optimisation* (Vol. 1). Springer Science & Business Media.

Chen, H. C., Chen, C. R., & Huang, K. (2013, June). CFD simulation of vortex-induced and wake-induced vibrations of dual vertical risers. In *Proc., 23rd Int. Offshore and Polar Engineering Conf*. Cupertino, CA: International Society of Offshore and Polar Engineers.

Chen, H. C., & Patel, V. C. (1988). Near-wall turbulence models for complex flows including separation. *AIAA journal*, *26*(6), 641-648.

Chen, H. C., & Patel, V. C. (1989). The flow around wing-body junctions. In *Symposium on Numerical and Physical Aspects of Aerodynamic Flows, 4th, Long Beach, CA* (p. 1989).

Chen, H. C., Patel, V. C., & Ju, S. (1990). Solutions of Reynolds-averaged Navier-Stokes equations for three-dimensional incompressible flows. *Journal of Computational Physics*, *88*(2), 305-336.

Gamino, M., Abankwa, S., & Pascali, R. (2013, June). FSI Methodology for Analyzing VIV on Subsea Piping Components With Practical Boundary Conditions. In *ASME 2013 32nd International Conference on Ocean, Offshore and Arctic Engineering* (pp. V007T08A028-V007T08A028). American Society of Mechanical Engineers.

Huang, K., Chen, H. C., & Chen, C. R. (2007, July). Riser VIV analysis by a CFD approach. In *Proceedings of the 17th International Offshore and Polar Engineering (ISOPE) Conference, Lisbon, Portugal*.

Huang, K., Chen, H. C., & Chen, C. R. (2008, July). Riser VIV induced fatigue assessment by a CFD approach. In *Proceedings of the 18th International Offshore and Polar Engineering (ISOPE) Conference, Vancouver, Canada*.

Huang, K., Chen, H. C., & Chen, C. R. (2011). Numerical scheme for riser motion calculation during 3-D VIV simulation. *Journal of Fluids and Structures*,*27*(7), 947-961.

Huang, K., Chen, H. C., & Chen, C. R. (2012). Vertical riser VIV simulation in sheared current. *International Journal of Offshore and Polar Engineering*, *22*(2), 142-149.

Lehn, E. (2003). VIV suppression tests on high L/D flexible cylinders (main report). *ExxonMobil upstream research company*.

Lucor, D., Imas, L., & Karniadakis, G. E. (2001). Vortex dislocations and force distribution of long flexible cylinders subjected to sheared flows. *Journal of Fluids and Structures*, *15*(3), 641-650.

Meakin, R. L. (1999). Composite overset structured grids. *Handbook of Grid Generation*, 1-20.

Meneghini, J. R., Saltara, F., de Andrade Fregonesi, R., Yamamoto, C. T., Casaprima, E., & Ferrari, J. A. (2004). Numerical simulations of VIV on long flexible cylinders immersed in complex flow fields. *European Journal of Mechanics-B/Fluids*, *23*(1), 51-63.

Newman, D., & Karniadakis, G. E. (1996). Simulations of flow over a flexible cable: a comparison of forced and flow-induced vibration. *Journal of fluids and structures*, *10*(5), 439-453.

Petersson, N. A. (1999). Hole-cutting for three-dimensional overlapping grids.*SIAM Journal on Scientific Computing*, *21*(2), 646-665.

Pontaza, J. P., Chen, C. R., & Chen, H. C. (2004). Chimera Reynolds-averaged Navier-Stokes simulations of vortex-induced vibration of circular cylinders. In*Civil Engineering in the Oceans VI* (pp. 166-176). ASCE.

Pontaza, J. P., Chen, C. R., & Chen, H. C. (2005, January). Simulations of high Reynolds number flow past arrays of circular cylinders undergoing vortex-induced vibrations. In *Proceedings of the 15th International Offshore and Polar Engineering (ISOPE) Conference* (pp. 201-207).

Pontaza, J. P., Menon, R. G., Swanson, R. C., Jhingran, V., Hill, M., Kopp, F., & Hoffman, J. (2010, January). Fluid-Structure interaction simulations of a pipeline span exposed to sea bottom currents. In *Offshore Technology Conference paper* (Vol. 21070).

Raghavan, K., Bernitsas, M. M., & Maroulis, D. E. (2009). Effect of bottom boundary on VIV for energy harnessing at $8\times 10^3 < Re < 1.5\times 10^5$. *Journal of Offshore Mechanics and Arctic Engineering*, *131*(3), 031102.

Suhs, N. E., & Tramel, R. W. (1991). *PEGSUS 4.0 User's Manual* (No. AEDC-TR-91-8). ARNOLD ENGINEERING DEVELOPMENT CENTER ARNOLD AFS TN.

Tognarelli, Michael A., Samuel Taggart, and Mike Campbell. "Actual VIV fatigue response of full scale drilling risers: with and without suppression devices." *ASME 2008 27th International Conference on Offshore Mechanics and Arctic Engineering*. American Society of Mechanical Engineers, 2008.

Trim, A. D., Braaten, H., Lie, H., & Tognarelli, M. A. (2005). Experimental investigation of vortex-induced vibration of long marine risers. *Journal of fluids and structures*, *21*(3), 335-361.

Tsahalis, D. T. (1983). The Effect of Seabottom Proximity of the Vortex-Induced Vibrations and Fatigue Life of Offshore Pipelines. *Journal of Energy Resources Technology*, *105*(4), 464-468.

Tsahalis, D. T. (1984). Vortex-induced vibrations of a flexible cylinder near a plane boundary exposed to steady and wave-induced currents. *Journal of Energy Resources Technology*, *106*(2), 206-213.

Tsahalis, D. T., & Jones, W. T. (1981, January). Vortex-Induced Vibrations Of A Flexible Cylinder Near A Plane Boundary In Steady Flow. In *Offshore Technology Conference*. Offshore Technology Conference.

Tsukada, R. I., & Morooka, C. K. (2013, June). A Numerical Simulation Procedure for Vortex-Induced Vibration of Pipelines With Free Span. In *ASME 2013 32nd International Conference on Ocean, Offshore and Arctic Engineering*(pp. V007T08A057-V007T08A057). American Society of Mechanical Engineers.

Veritas, D. N. (2006). Recommended Practice DNV-RP-F105. *Free spanning pipelines*.

Yang, B., Gao, F. P., Jeng, D. S., & Wu, Y. X. (2008). Experimental study of vortex-induced vibrations of a pipeline near an erodible sandy seabed. *Ocean engineering*, *35*(3), 301-309.